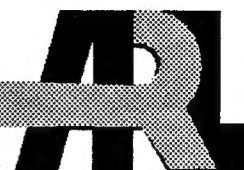


ARMY RESEARCH LABORATORY



# Improved Tungsten Penetrators

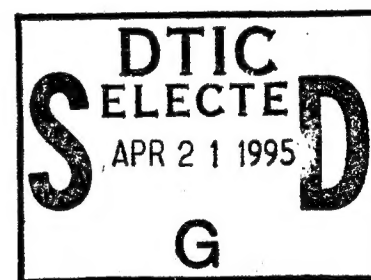
Ward Stevens and Patrick Lang

ARL-CR-177

September 1994

**Prepared by**  
Advanced Technology Materials  
7 Commerce Drive  
Danbury, CT 06810

**under contract**  
DAAL01-93-C-4006



19950420 016

DTIC QUALITY INSPECTED 5

# DISCLAIMER NOTICE



THIS DOCUMENT IS BEST QUALITY AVAILABLE. THE COPY FURNISHED TO DTIC CONTAINED A SIGNIFICANT NUMBER OF COLOR PAGES WHICH DO NOT REPRODUCE LEGIBLY ON BLACK AND WHITE MICROFICHE.

The findings in this report are not to be construed as an official Department of the Army position unless so designated by other authorized documents.

Citation of manufacturer's or trade names does not constitute an official endorsement or approval of the use thereof.

Destroy this report when it is no longer needed. Do not return it to the originator.

REPORT DOCUMENTATION PAGE			Form Approved OMB No. 0704-0188	
Public reporting burden for this collection of information is estimated to average 1 hour per response, including the time for reviewing instructions, searching existing data sources, gathering and maintaining the data needed, and completing and reviewing the collection of information. Send comments regarding this burden estimate or any other aspect of this collection of information, including suggestions for reducing this burden, to Washington Headquarters Services, Directorate for Information Operations and Reports, 1215 Jefferson Davis Highway, Suite 1204, Arlington, VA 22202-4302, and to the Office of Management and Budget, Paperwork Reduction Project (0704-0188), Washington, DC 20503.				
1. AGENCY USE ONLY (Leave blank)		2. REPORT DATE September 1994		3. REPORT TYPE AND DATES COVERED Final Report, 2/23/93 - 8/23/93
4. TITLE AND SUBTITLE Improved Tungsten Penetrators - SBIR			5. FUNDING NUMBERS Contract No. DAAL01-93-C-4006	
6. AUTHOR(S) Ward Stevens and Patrick Lang				
7. PERFORMING ORGANIZATION NAME(S) AND ADDRESS(ES) Advanced Technology Materials 7 Commerce Drive Danbury, CT 06801			8. PERFORMING ORGANIZATION REPORT NUMBER OB5Y0	
9. SPONSORING/MONITORING AGENCY NAME(S) AND ADDRESS(ES) U.S. Army Research Laboratory Watertown, MA 02172-0001 ATTN: AMSRL-OP-PR-WT			10. SPONSORING/MONITORING AGENCY REPORT NUMBER ARL-CR-177	
11. SUPPLEMENTARY NOTES R. Dowding, COR				
12a. DISTRIBUTION/AVAILABILITY STATEMENT Approved for public release; distribution unlimited.			12b. DISTRIBUTION CODE	
13. ABSTRACT (Maximum 200 words) Kinetic energy penetrators composed of tungsten based alloys avoid the cost and toxicity issues associated with uranium. In this program, High Pressure Float Zone crystal growth was investigated as a means of producing single crystal and oriented polycrystalline tungsten and tungsten alloys. X-ray diffraction, high rate compression testing, and optical microscopy were used to assess the results. Attempts to float zone pure tungsten were unsuccessful because the high powers required to melt tungsten resulted in electrical arcing between the sample and the induction coil. Lowering the melting temperature through alloying with nickel, iron, and rhenium proved successful and in certain cases resulted in elongated grains. In most cases the high rate compression test results were similar to most tungsten alloys reported elsewhere; the samples showed strain hardening. While polycrystalline tungsten rods produced with a traveling nickel-iron molten zone showed some signs of softening, each of these samples rubblized during testing. Further work would be required to determine the nature of these samples microstructural response and any benefits to penetrator performance. Samples of each material were delivered to the Army for further testing.				
14. SUBJECT TERMS Tungsten, Single crystals, Solidification Tungsten alloys, Floating zone			15. NUMBER OF PAGES 43	
			16. PRICE CODE	
17. SECURITY CLASSIFICATION OF REPORT Unclassified	18. SECURITY CLASSIFICATION OF THIS PAGE Unclassified	19. SECURITY CLASSIFICATION OF ABSTRACT Unclassified	20. LIMITATION OF ABSTRACT UL	

## Table of Contents

	Page
1. Introduction and Background	1
2. Phase I Technical Objectives	2
3. Phase I Technical Review	3
3.1 Experimental Overview	3
3.2 Task 1 Float zone crystal growth of tungsten	4
3.3 Task 2 Liquid phase sintering of W-Ni-Fe CIP rods	5
3.4 Task 3 Float zone growth of tungsten using Ni-Fe molten zone	7
3.5 Task 4 Production of tungsten with 5% rhenium	8
3.6 Task 5 Characterization of the tungsten samples	9
4. Program Summary and Recommendations	10
5. References	11

## List of Tables

Table 1. Penetrator Results of Bruchey and Coworkers	12
Table 2. Dynamic Compression Results	12

Accession For	
NTIS CRA&I	<input checked="" type="checkbox"/>
DTIC TAB	<input type="checkbox"/>
Unannounced	<input type="checkbox"/>
Justification _____	
By _____	
Distribution /	
Availability Codes	
Dist	Avail and/or Special
A-1	

## List of Figures

	Page
1a. TSS High Pressure Float Zone Apparatus	13
1b. Tungsten float zone set up	13
2a. Laue pattern for outer edge of float zoned tungsten rod	14
2b. Diffraction pattern for outer edge of float zoned tungsten rod	14
3a. Cross section float zoned tungsten rod	15
3b. Long section float zoned tungsten rod	15
3c. Long section float zoned tungsten rod- out side	16
4. Long section float zoned tungsten- inside	16
5. Long section unheated tungsten rod	17
6a. Long section of CIP rod translated 1"/hr at 1500°C	17
6b. Long section CIP rod translated 1/4"/hr at 1200°C	18
7. Long section CIP rod, 1"/hr at 1200°C	18
7a. Edge CIP rod 1/4"/hr at 1200°C	19
7b. CIP rod 1"/hr at 1200°C	19
7c. CIP rod translated 1"/hr at 1200°C	20
7d. X-ray diffraction sintered CIP rod	20
8. Float zone attempt with 86% W CIP rod	21
9. Ingot #4, sintered and float zoned 93% W CIP rod	21
10. X-ray diffraction of tip of ingot #4	22
11. Ingots of 93% W sintered & float zoned before EDM	22
12a. Compression sample 4-1- made from ingot #4	23
12b. Compression sample 4-1- made from ingot #4	23
12c. Compression sample 4-2- made from ingot #4	24
12d. Compression sample 4-2- made from ingot #4	24
12e. Compression sample 4-3- made from ingot #4	25
12f. Compression sample 4-3- made from ingot #4	25
13. Samples 4-1, 4-2, 4-3 after compression testing	26
14. Ingot 2W, float zoned W rod with Ni-Fe molten zone	26
15a. X-ray diffraction ingot 2W center of tip	27
15b. Laue pattern ingot 2W	27
16a. Compression sample 2W-1- made from ingot 2W	28

### List of Figures (continued)

	Page
16b. Compression sample 2W-1- made from ingot 2W	28
16c. Compression sample 2W-2- made from ingot 2W	29
16d. Compression sample 2W-2- made from ingot 2W	29
16e. Compression sample 2W-3- made from ingot 2W	30
16f. Compression sample 2W-3- made from ingot 2W	30
17. Samples 2W-1, 2W-2, 2W-3 after compression testing	31
18. Ingots made by sintering & float zoning CIP rods with 5% Re	31
19. Center of tip of ingot 2R	32
21a. Compression sample 2R-1- made from ingot 2R	32
21b. Compression sample 2R-1- made from ingot 2	33
21c. Compression sample 2R-2- made from ingot 2R	33
21d. Compression sample 2R-2- made from ingot 2R	34
21e. Compression sample 2R-3- made from ingot 2R	34
21f. Compression sample 2R-3- made from ingot 2R	35
22. Sample 2R-1, 2R-2, 2R-3 after compression testing	35
23a. Compression and ballistic samples- 93% W CIP rods after EDM.	36
23b. Compression & ballistic samples from W-Re CIP rods after EDM	36
23c. Compression and ballistic samples, pure W rods after EDM	37

## 1. Introduction and Background

Kinetic energy penetrators are currently relied upon as a way to defeat enemy armor. Historically these penetrators have been composed of uranium or tungsten based alloys due to their high densities. In addition to density, the deformation behavior of the alloy determines its performance. A penetrator whose tip mushrooms or fractures on impact is less effective than a penetrator that retains its shape or has a tip that self sharpens. Although the densities of uranium and tungsten are similar, uranium alloys have generally exhibited deformation on impact that has resulted in better penetrator performance. The drawbacks with uranium alloys, however, are toxicity and cost.

Recent work by Bruchey and coworkers<sup>1,2</sup> indicated that single crystals of pure tungsten, oriented in the  $\langle 100 \rangle$  direction, performed as well as depleted uranium in laboratory ballistic experiments. Bruchey attributed this behavior to the favorable orientation of the four  $[111]$  slip planes available for dislocation motion. Tungsten crystals oriented in the  $\langle 111 \rangle$  direction and  $\langle 110 \rangle$  direction, and polycrystalline penetrators composed of 93% tungsten with nickel and iron did not penetrate as deeply into a block of steel. Table 1, from Bruchey, summarizes his results.

This work showed that tungsten based materials have the potential to give penetrator performance that rivals that of uranium based materials. The problem lies in the production of large oriented single crystals of tungsten. The maximum size of tungsten crystals now available is less than 10 mm in diameter. Diameters of 10 mm are needed for 1/4 scale laboratory testing, and diameters of 40 mm are needed for full scale penetrators.

The difficulty in tungsten single crystal growth can be traced to its high melting temperature. At temperatures greater than tungsten's  $3410^{\circ}\text{C}$  melting temperature, crucibles that do not react with or contaminate the melt are nonexistent. If the Czochralski crystal growth technique is used, where a single crystal is slowly pulled from a bath of molten tungsten, the tungsten must be contained by a "crucible" of tungsten which is prevented from melting by water cooling. A large amount of power is required to maintain

the  $>3410^{\circ}\text{C}$  melt temperature. Heat losses by radiation from the surface of the melt are significant. Heat losses by conduction through the water cooled tungsten crucible are also great due to tungsten's relatively high thermal conductivity. Whether the power is supplied by induction, resistance heating of the tungsten, or by radiation such as with a laser, controlling the thermal gradients within the tungsten melt is a difficult problem. This problem undoubtedly contributes to the current size limitations of tungsten crystals.

Because of tungsten's high melting point and thermal loss problems, a "crucible-less" technique is preferred for crystal growth. High pressure float zone (HPFZ) crystal growth is one of the few options for growing tungsten single crystals. In this technique, recrystallization occurs through a rod-shaped preform as a heated molten zone is passed through the rod. For over four years ATM has had an active program to grow single crystals of refractory carbides by float zone. This experience was brought to bear on the related problem of tungsten crystal growth.

In this Phase I SBIR program, tungsten alloys were produced with modifications to the float zone process in an attempt to improve their performance as penetrators. ATM sought to produce large ( $>10$  mm diameter) [100] oriented crystals of pure tungsten and W-Ni-Fe alloy rods with elongated and preferred orientation of the grains. Float zone modifications that could produce material of the quality required for penetrators were explored. X-ray diffraction, high rate compression testing, and optical microscopy were used to assess the results.

## **2. Phase I Technical Objectives**

The objectives of this Phase I program included:

1. The growth of 10 mm diameter by 100 mm long single crystals of tungsten by modified float zone.
2. Liquid phase sintering W-Ni-Fe to obtain an elongated and/or preferred orientation grain structure.

3. The production of tungsten with an elongated and/or preferred orientation grain structure using a Ni-Fe float zone.
4. An assessment of the effect of rhenium on penetrator performance.

### **3. Phase I Technical Review**

#### **3.1 Experimental Overview**

The Phase I work plan called for the completion of six tasks:

1. Float zone crystal growth of tungsten.
2. Liquid phase sintering W-Ni-Fe.
3. Float zone crystal growth of tungsten using a Ni-Fe molten zone.
4. Production of tungsten with 5 % rhenium.
5. Characterization of tungsten samples.
6. Final report preparation.

To improve tungsten penetrators attempts were made to produce 1/4 scale ballistic samples which were single crystals, showed preferred orientation, or had longitudinally elongated grain structures. Float zoning and sintering was done with a TSS High Pressure Float Zone apparatus designed to grow refractory crystals (Figure 1a). The apparatus has a water cooled furnace chamber that can be pressurized to 1000 psi where samples are heated by passing them vertically through a multi-turn water cooled induction coil (Figure 1b). The samples can be held by top and bottom water cooled grips. These grips can be translated and rotated synchronously. The vertical travel limit for this apparatus is six inches, and pulling speeds can be varied from 0.03 to 60 inches per hour. Power was supplied by a 100 KW Lepel RF power supply.

Task 5 called for the analysis of the samples made. Metallographic sections were obtained by cutting with a low speed diamond saw. These sections were embedded in epoxy and polished with a Buehler automatic grinder/polisher. The polishing protocol used successively smaller size diamond slurries and wheels ending with Murakami's solution with alumina. Final development of grain structure was accomplished by etching in Murakami's solution for

several hours. Optical microscopy of the samples was performed with an Olympus Stereomicroscope, and an Olympus reflected light microscope both equipped with a Polaroid film camera. X-ray analysis of samples was done with a Rigaku x-ray diffractometer. Ballistic samples were produced, machined, and delivered to the Army and to Southwest Research Institute (SwRI) for compression testing. SwRI used a split Hopkinson pressure bar apparatus for compressive loading at high dynamic rates. The experiments and results of each task are given below.

### 3.2 Task 1 Float zone crystal growth of tungsten.

Several attempts were made to float zone 100% dense tungsten in hopes of producing a single crystal. A 6 inch long by 1/2 diameter tungsten rod obtained from GTE Sylvania was held in the upper grip. A second rod, 1 inch in length, was held in the lower grip such that it just touched the upper rod. An induction coil, 1/2 inch inner diameter with two triple turn pancakes was positioned at the point where the two rods met. Preliminary trials showed that excessive heat losses prevented the formation of a molten zone. In an attempt to reduce the heat loss down the rod and through the water cooled grips, the rod was cut with 1/8 inch deep slots. These slots were perpendicular to the long axis of the rod, offset by 120°, and spaced at 3/4 inch intervals along the rod (Figure 1b).

The furnace was pressurized with high purity helium at 500 psi to inhibit arcing. A 200 KHz RF frequency was used to heat the rods. When a molten zone was established travel was started; a synchronous travel rate of 1/4 inch per hour was used to move the rods downward. The rods were moved down for about two hours with moderate arcing between the coil and the rods. After about a 1/2 inch of travel, a large arc was experienced which perforated the water cooled copper induction coil and shut down the power source. Another attempt was made, but with the power source modified to yield a frequency of 180 KHz. After about an hour of travel arcing again stopped the run. Subsequent attempts with larger diameter coils resulted in lower coupling efficiency, higher voltages and greater arcing. Coils with different configurations and numbers of turns did not eliminate arcing.

The two small float zone areas of pure 100% dense tungsten rods were sectioned polished and etched for optical microscopy. They were also subjected to x-ray analysis. The rocking curves and Laue patterns indicated preferred crystal orientation on the outside of the sample, but not in the center (Figure 2). Optical microscopy showed two distinct areas, an inner area with definite longitudinal grain elongation and an outer area with more equi-axed grains (Figure 3). It is apparent that the rod was not melted completely through. Comparison of this central area (Figure 4) with the as-received rod (Figure 5) suggests that the interior of the rod experienced some grain growth during the float zone attempt. This suggests that high temperature treatment could preserve or improve an elongated grain structure without going up to the melting temperature of 3410°C. Since the power levels could then be reduced, the propensity for arcing might also be reduced.

Single crystal tungsten rods could be produced if the arcing problem could be eliminated. Further experimentation with different grips, designed to reduce heat loss, and lower frequency power sources could make single crystal production feasible.

### 3.3 Task 2 Liquid phase sintering of W-Ni-Fe CIP rods

Cold isostatically pressed (CIP) rods were liquid phase sintered in an attempt to produce preferred orientation and/or longitudinally elongated grain structures for improved penetrator performance.<sup>3</sup> High purity, high density, small grain sizes were needed in the preformed rods. Powders of 99.5% purity and -325 mesh particle size were pressed at 45,000 psi to yield a density of 62%. Twenty-eight samples of various compositions were pressed into rods at Gorham Advanced Materials Laboratories. These rods were around 150 mm in length and 15 mm in diameter. Fourteen of the CIP rods were 93% W-4.9% Ni-2.1% Fe, seven were 86% W-9.8% Ni-4.2% Fe, and seven were 88% W-4.9% Ni-2.1% Fe-5% Re.

Different induction coil configurations, temperatures, travel directions, and translation rates were tried in an effort to find the best way to sinter the CIP rods. The densest, 93% W, CIP rods were found to sinter best. These rods

were held by the top grip and translated down through the induction coil using a frequency of 200 KHz with 500 psi high purity helium. It was found that a two turn single pancake 1/2 inch ID coil performed best. A translation rate of 1/4 inch per hour and a temperature of 1200°C (optical pyrometer) kept volatilization to a minimum, and samples produced in this manner showed minimal residual porosity between grains, and good contiguity (Figure 6). The sintered rods were examined similarly to the pure tungsten rods using optical microscopy and x-ray analysis.

Grain elongation was seen on the outside skin of the rods; however, there was none of the hoped for longitudinally elongated grains except in some small areas (Figure 7). The lack of orientation in the interior could have been due to the lower thermal conductivity of the CIP rods which could hinder interior cooling. A smaller temperature gradient along the rod was noted as it passed down through the coil. Since the skin temperature cools more rapidly than the interior, grain elongation was radial at the skin (Figure 7a). At high translation rates residual porosity was great and dendrite formation at the skin was noted, an indication of super-cooling (Figure 7b). The interior also showed porosity, but lacked the dendrites seen in the skin (Figure 7c). X-ray analysis showed evidence of high narrow peaks indicating some preferred orientation in the interior (Figure 7d).

Attempts were also made to float zone the CIP rods. The apparatus was pressurized with high purity helium gas to 500 psi. The CIP rod was held in the top grip and a 1 inch long pure tungsten rod held in the bottom grip. The two rods were brought together inside a three turn double pancake 1/2 inch coil. A molten zone was established and maintained as the rods were translated downward.

First float zone attempts were made with 86% tungsten because of its higher nickel-iron content and consequent lower melting temperature. The greater amounts of nickel and iron resulted in more volatilization. When the molten zone was translated alternate melting and freezing occurred, presumably a result of the loss of lower melting components. Increasing and decreasing the power to the coils to compensate for this led to overheating and overflow of

the molten zone (Figure 8). This problem was reduced with 93%W rods, but float zoning was still not satisfactory.

To overcome instabilities in float zoning, the green 93% W rods were first sintered, as in Task 2, to increase their density, and then were float zoned. This method proved to be best for producing low porosity, high contiguity, and longitudinal grain elongation (Figure 9). X-ray diffraction suggest random orientation (Figure 10) as all peaks correspond to powder profiles. While the microstructure was improved, processing time increased; this sample required twenty hours to process. Three ingots for ballistic samples and one for compression samples were made following this procedure (Figure 11) and were sent out for machining and testing.

Compression testing performed by SwRI showed ultimate strains between 25 and 30% for all test samples made from CIP rods. True compressive strengths for these samples were uniform, about 215 Ksi (Table 2). These compression samples also showed systematic plastic deformation across the entire gauge length (Figure 12) and no cracking was apparent (Figure 13).

#### 3.4 Task 3 Float zone crystal growth of tungsten using Ni-Fe molten zone.

To lower the temperature needed to float zone pure tungsten, an attempt was made to produce float zoned pure tungsten rods using a moving Ni-Fe molten zone. Molten nickel-iron alloys with tungsten, lowers its melting temperature. This alloyed material travels along the rod as it moves through the coil. A nickel-iron molten zone was used between two pure tungsten rods with the 5 inch long upper rod float zoned as it passed down through three turn double pancake 1/2 inch coil. Nickel and iron slugs cut from pure nickel and iron rods, in a seven to three mass ratio, respectively, were placed on top of a lower 1 inch long tungsten rod. The lower rod was brought up until the tip supporting the nickel and iron slugs was inside the coil. The rod that was to be float zoned was held by the top grip and was lowered to be in contact with the nickel and iron slugs.

A molten zone was established between the two rods as they were moved through the coil at 0.6 inches per hour. The temperature was adjusted to

insure complete melting through the rod. Again, because of the high thermal conductivity of the tungsten, both the upper and lower rods had 1/8 inch deep slots cut every inch, offset by 120° around the circumference. These slots were cut at right angles to the long axis of the rod and were necessary to prevent arcing. After about an hour of travel as the molten zone passed over the first slot it began to freeze. This was due to the loss of the nickel and iron by volatilization and the narrowing of the rod. The temperature was raised and the translation rate slowed to 1/4 inch per hour but the molten zone did not appear to be all the way through the rod. Microscopic analysis of the cross and longitudinal sections showed large, elongated, contiguous grains with no porosity near the tip (Figure 14). It appears that this method of producing ingots with the desired properties has promise. Three ballistic samples ingots, and one compression samples ingot made by this method were sent out for machining and testing. Unfortunately some residual slots were left after machining the ballistic samples. The absence of major peaks in diffraction analysis suggests preferred orientation, but preliminary Laue analysis was not confirming (Figure 15).

In the compression testing by Southwestern Research institute ultimate strains for the these samples were well below those of the samples made from CIP rods.(see figure 16) The samples made by nickel iron float zoning pure tungsten rod were rubblized at these lower strain levels (Figure 17). True compressive strengths for these samples ranged from around 240 to 249 Ksi (Table 2).

### 3.5 Task 4 Production of tungsten with 5% rhenium.

The same sinter/float zone method used to densify and melt the 93% W CIP rods was used to produce samples of W 5%Re. Three ballistic samples ingots and one compression samples ingot were made and sent for testing (Figure 18). It was noted that these ingots were difficult to cut with the diamond saw. Like the ingots made from 93% W CIP rods, the Re containing CIP rods showed low porosity, high contiguity, and longitudinal grain elongation (Figure 19).

Compression testing by SwRI showed ultimate strains between 25 and 30% for all test samples made from Re containing CIP rods. True compressive strengths for these samples were between 209 and 218 Ksi (Table 2). The compression samples also showed systematic plastic deformation across the entire gauge length (Figure 20) and no cracking was seen (Figure 21).

### 3.6 Tasks 5 Characterization of the tungsten samples.

Optical microscopy and x-ray diffraction analysis was used on all samples made. Ingots were sectioned across and along the long axis of the rod by cutting with a diamond saw. These sections, encased in hardened resin, were ground and polished with diamond wheels and paste in a polishing protocol that finished with 0.05 micron alumina in Murakami's solution and then etched in the solution for several hours to develop the grain structure. The results of these analyses are given in the section on each task.

The twelve ingots made were sent out for EDM machining into three 1/2 inch by 4 inch ballistic samples and three 1/2 inch by 1/4 inch compression samples for each method (Figure 22). Ballistic samples were delivered to R. Dowding at the Army Research facility in Watertown, Mass.

Compression samples were sent to Southwest Testing Laboratory. The nine tungsten compression samples were tested in a split Hopkinson pressure bar system. Loading pulses were generated with a seven-inch striker bar and yielded strain rates in the range of approximately  $3600\text{s}^{-1}$  to just in excess of  $4000\text{s}^{-1}$ . The results are given in the section on each task. With the exception of material processed with a nickel-iron molten zone, all samples showed barreling and typical (true stress-true strain) strain hardening behavior.<sup>4,5</sup> While the data for samples made using the nickel-iron molten zone shows what appears to be softening under dynamic testing, all of these samples rubblized. When rubblization occurred and its importance to the apparent "softening" are not known, but warrants further investigation.

#### 4. Program Summary and Recommendations

Attempts to produce single crystals of tungsten were unsuccessful in this program. The power levels were too great given the coil configuration and the frequency available with the equipment used; the high power resulted in catastrophic arcing between the coil and the sample. These circumstances can be remedied through lower frequency power and by employing insulated grips to avoid heat loss through the specimen.

Lowering the melting temperature through alloying with nickel, iron, and rhenium proved successful; several ingots of polycrystalline tungsten were produced. Protocols were established for cold isostatically pressing alloy preforms, densifying the preforms with a traveling coil, and finally float zoning the densified preforms.

The use of a traveling nickel-iron molten zone was also useful in establishing a molten zone and float zoning a tungsten rod. Simply by placing a nickel-iron slug between two tungsten rods was sufficient to enable complete melting without arcing. X-ray results on materials produced by the traveling molten zone technique showed some indication of preferred orientation. Similarly optical microscopy indicated that elongated grains were present in these materials.

In most cases the high rate compression test results were similar to most tungsten alloys reported elsewhere; the samples showed strain hardening. While polycrystalline tungsten rods produced with a traveling nickel-iron molten zone showed some signs of softening, each of these samples rubblized during testing. Further work would be required to determine the nature of these samples microstructural response and any benefits to possible penetrator performance. Samples of each material produced were delivered to the Army for further testing.

## 5. References

1. Bruchey, W. J., et. al., "Deformation Mechanisms in Tungsten Single Crystals in Ballistic Impact Experiments," *High Strain Rate Behavior of Refractory Metals and Alloys*, ed. Aafahani, TMS 1992 145-155.
2. Bruchey, W. J., et. al., "Orientation Dependence of Deformation and Penetration Behavior of Tungsten Single Crystal Rods," *Tungsten and Tungsten Alloys: Recent Advances*, Eds A. Crowson and E. Chen, TMS, 1991 p.121-128.
3. German, R. M., *Liquid Phase Sintering*, Plenum, New York, 1985.
4. Lankford, J., Jr., Couque, H., Bose, A., and German, "Dynamic Deformation and Failure of Tungsten Heavy Alloys", *Tungsten and Tungsten Alloys: Recent Advances*, Eds A. Crowson and E. Chen, TMS, 1991,p.151.
5. Couque, H., Lankford, J., Jr., and Bose, A., "Tensile Fracture and Shear Localization Under High Loading Rate in Tungsten Alloys", *Jr. Phys. III FRANCE 2, No. 11*, 1992, p.29.

**Table 1. Penetrator Results of Bruchey and Coworkers<sup>1,2</sup>**

<u>Material</u>	<u>Penetration/Unit Rod Length</u>
93W-Ni-Fe Ordnance Alloy	0.84
U-0.75Ti Ordnance Alloy	0.95
<111> W Single Crystal	0.88
<110> W Single Crystal	0.83
<100> W Single Crystal	0.97

**Table 2. Dynamic Compression Results.**

Samples labeled "4" are 93%W CIP rods sintered and float zoned, "2W" samples are made from pure tungsten rods float zoned with Ni-Fe molten zone, "2R" samples are from CIP rods containing Re.

Specimen No.	Diameter (in.)	Length (in.)	Area (x10 <sup>-2</sup> in <sup>2</sup> )	$\dot{\epsilon}$ (sec <sup>-1</sup> )	$\sigma_U$ True (Ksi)
4-1	0.2505	0.5016	4.928	3814.70	214.983
4-2	0.2504	0.5016	4.924	3816.12	214.021
4-3	0.2504	0.5007	4.924	3837.18	214.743
2W-1	0.2503	0.5008	4.921	3601.45	249.203
2W-2	0.2502	0.5018	4.917	4002.15	239.775
2W-3	0.2505	0.5021	4.928	4035.50	240.457
2R-1	0.2499	0.5017	4.905	3775.44	217.711
2R-2	0.2500	0.5018	4.909	3847.12	214.101
2R-3	0.2499	0.5007	4.905	3847.38	209.006

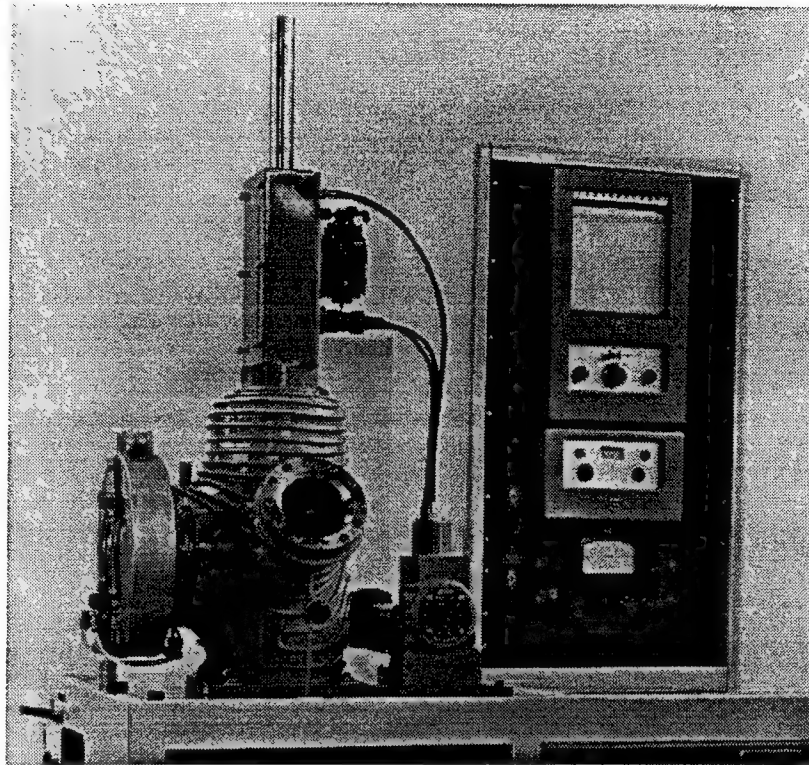


Figure 1a. TSS High Pressure Float Zone Apparatus

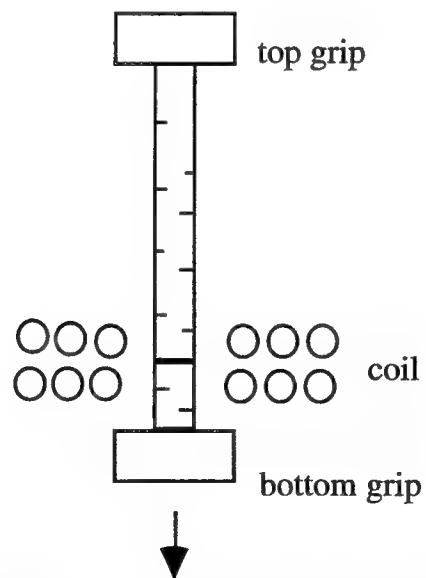


Figure 1b. Tungsten float zone set up.

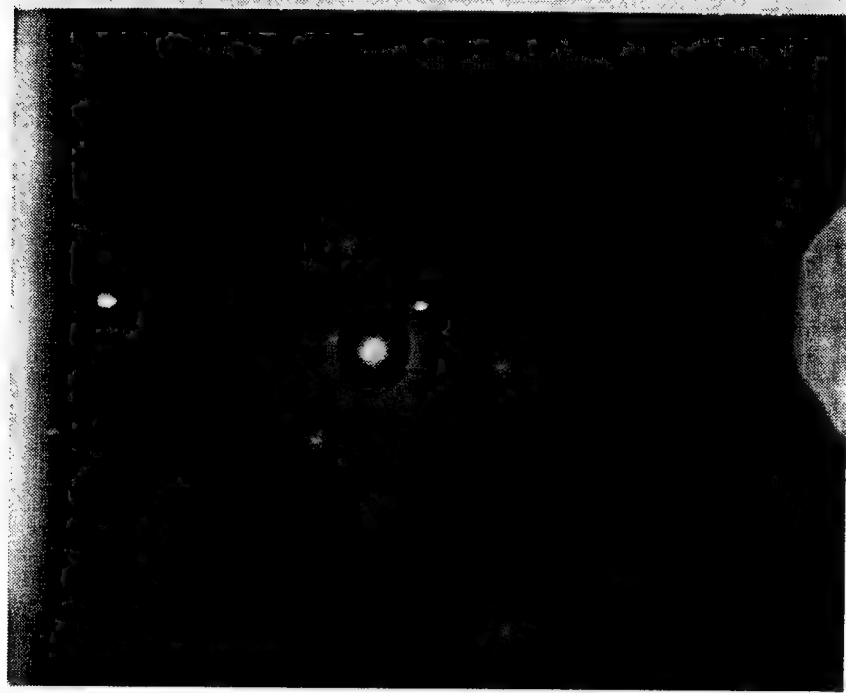


Figure 2a. Laue pattern for outer edge of float zoned tungsten rod.

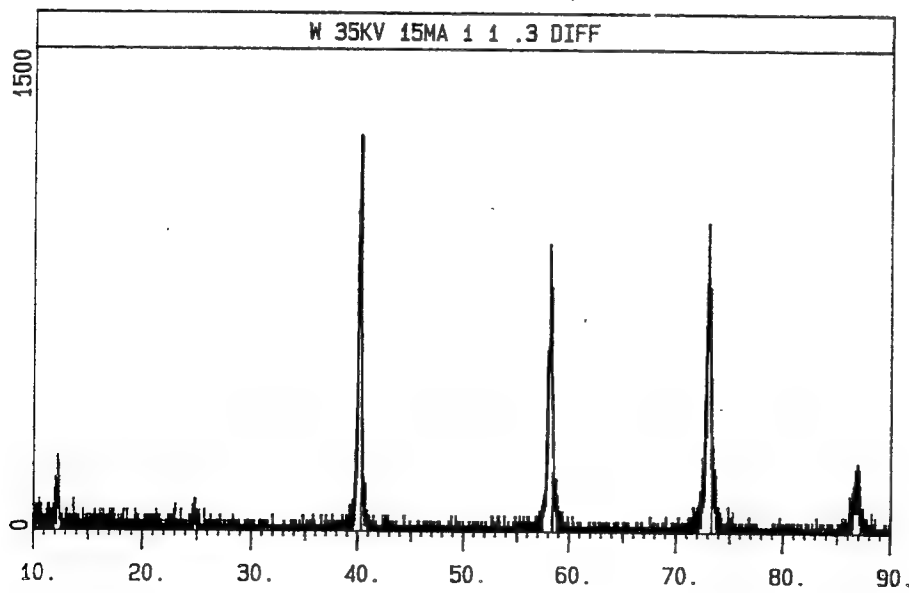


Figure 2b. Diffraction pattern for outer edge of float zoned tungsten rod.

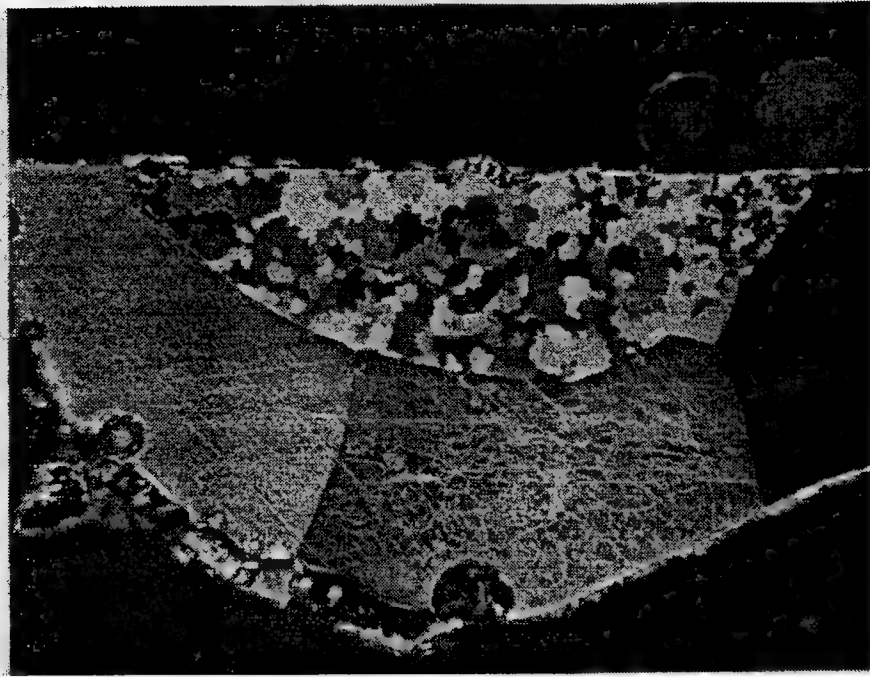


Figure 3a. Cross section float zoned tungsten rod. 10X

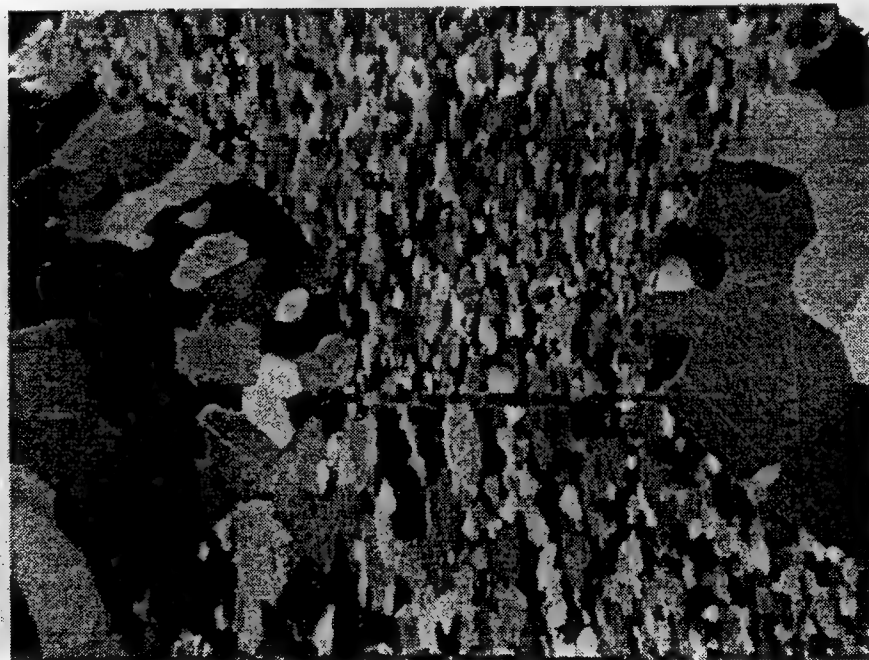


Figure 3b. Long section float zoned tungsten rod. 10X

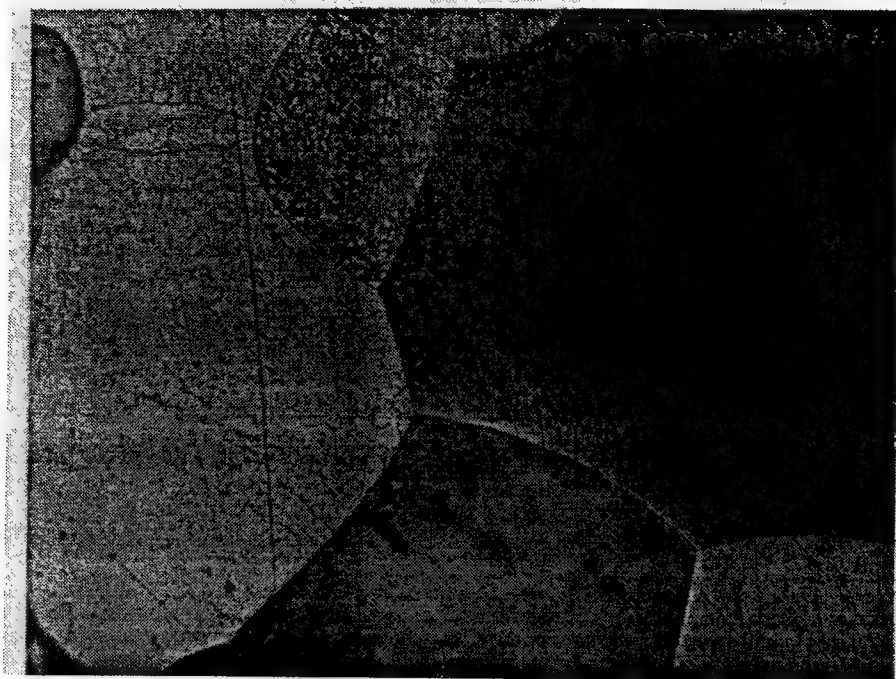


Figure 3c. Long section float zoned tungsten rod- out side. 50X

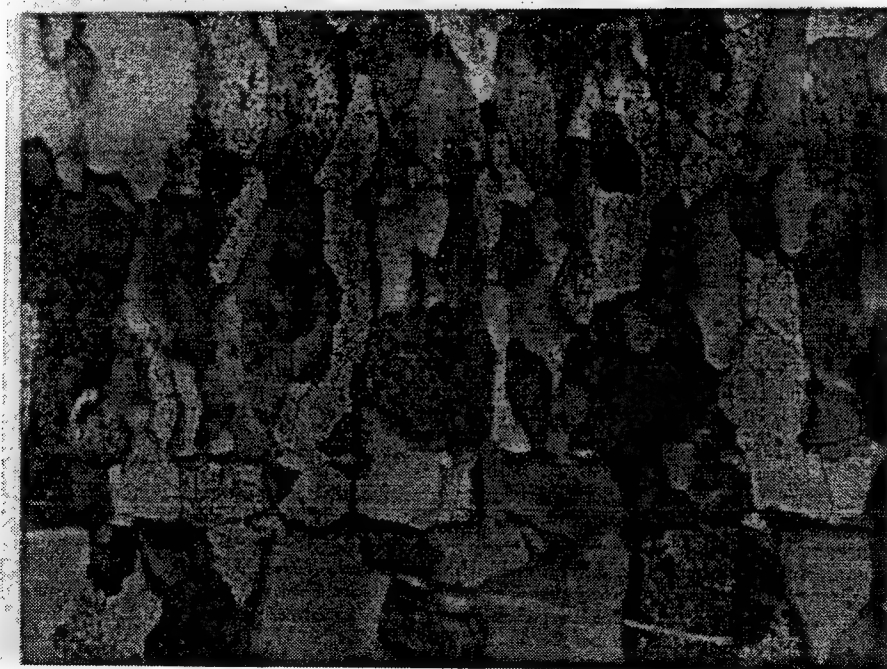


Figure 4. Long section float zoned tungsten- inside. 100X



Figure 5. Long section unheated tungsten rod.

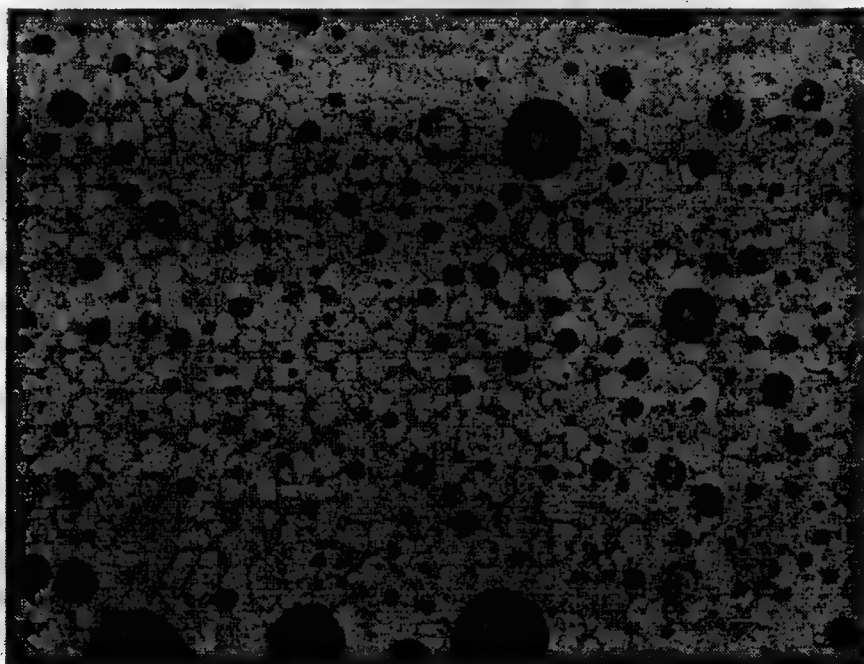


Figure 6a. Long section of CIP rod translated 1"/hr at 1500°C. 200X.

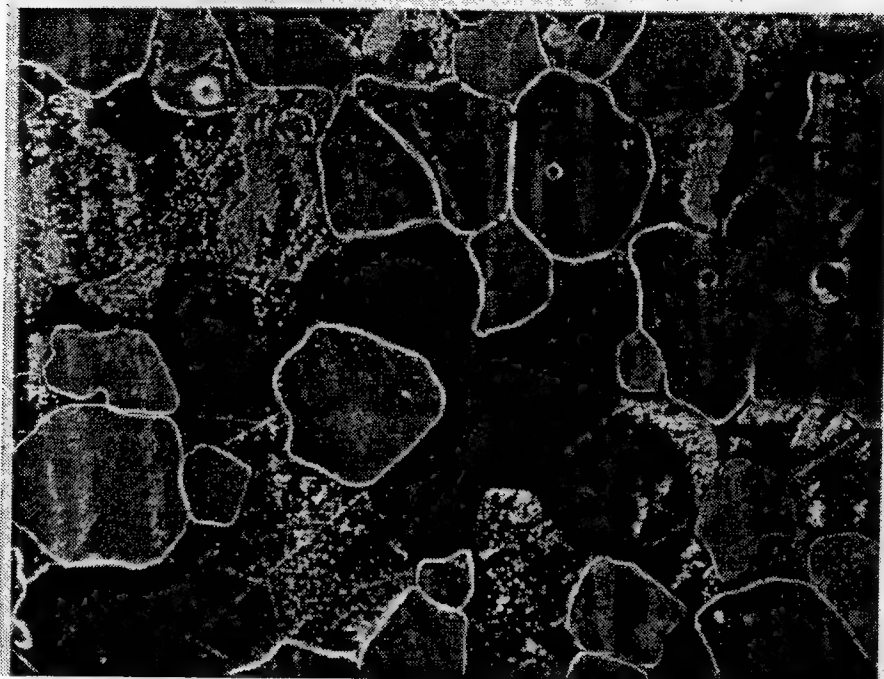


Figure 6b. Long section CIP rod translated 1/4"/hr at 1200°C. 200X

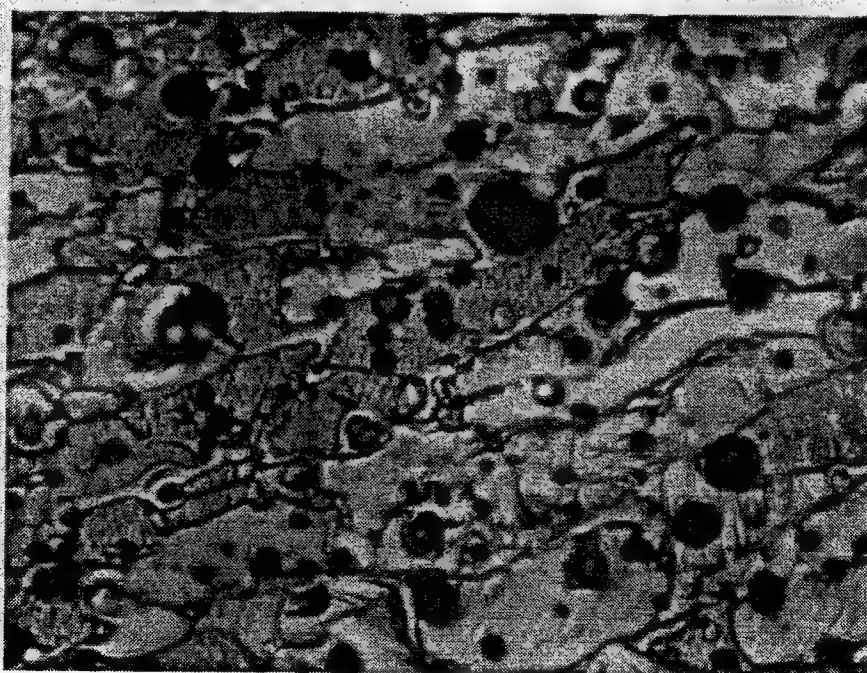


Figure 7. Long section CIP rod, 1"/hr at 1200°C- travel across page. 200X.



Figure 7a. Edge CIP rod 1/4"/hr at 1200°C- travel across page. 200X.

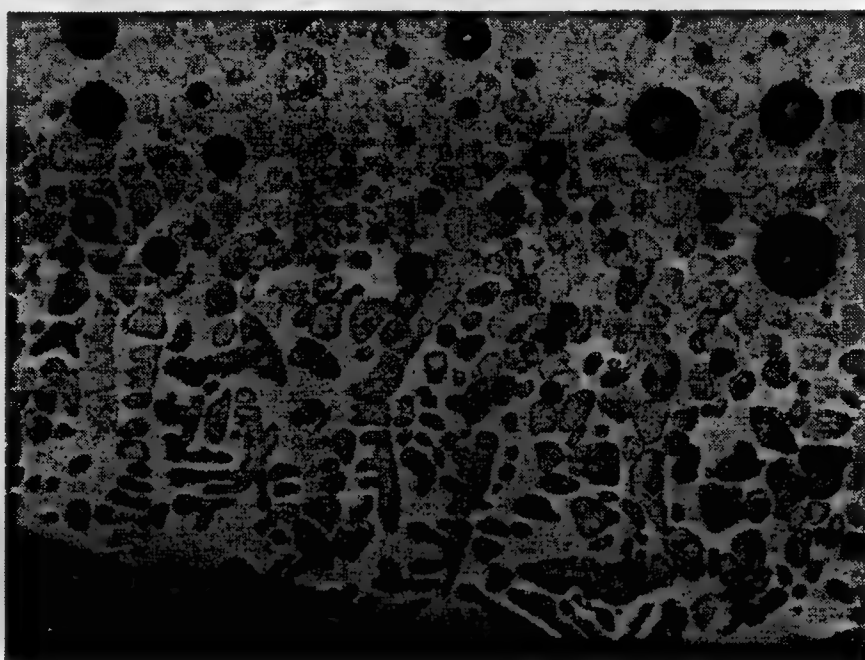


Figure 7b. CIP rod 1"/hr at 1200°C- travel across page. 200X.

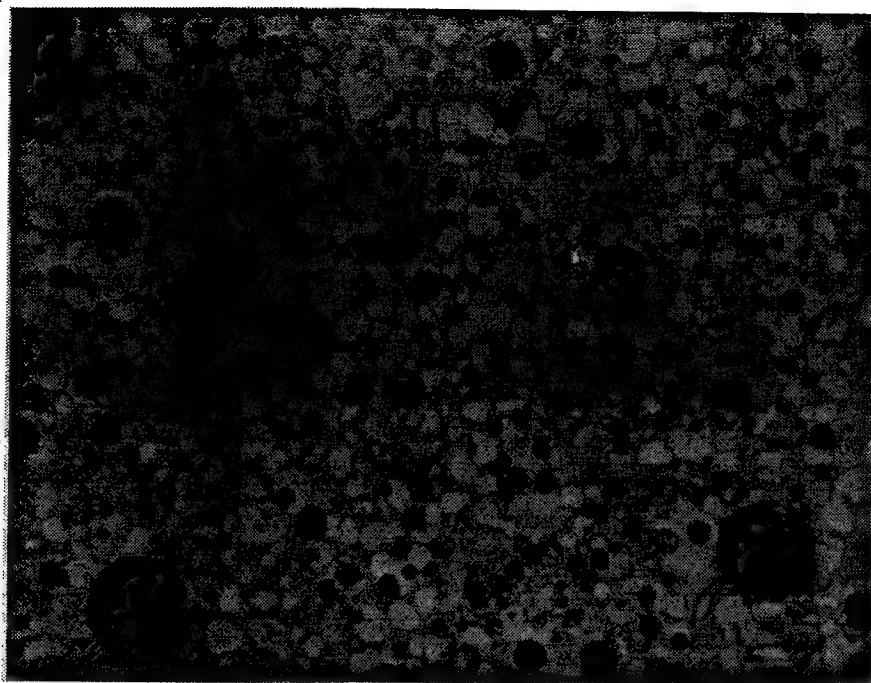


Figure 7c. CIP rod translated 1"/hr at 1200°C- travel across page. 200X.

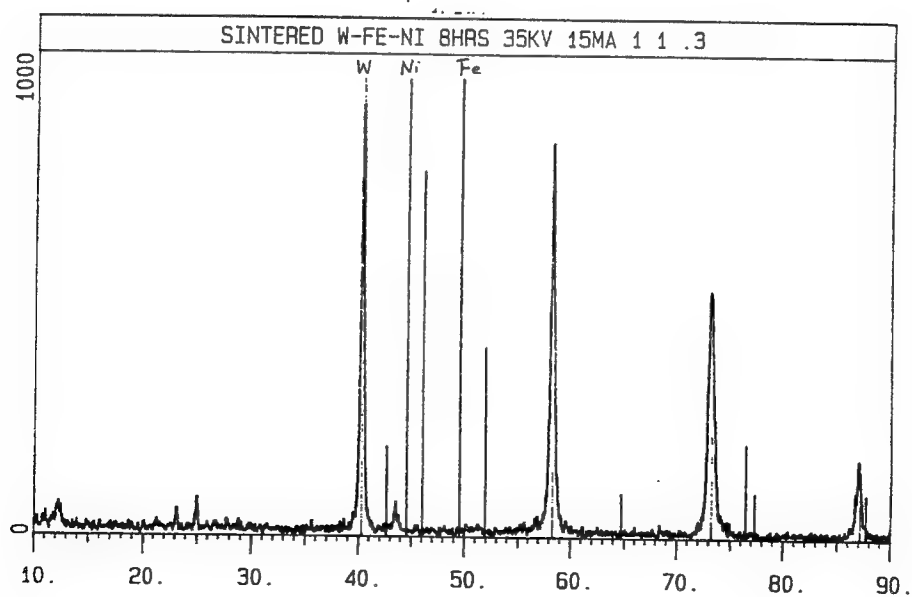


Figure 7d. X-ray diffraction sintered CIP rod.

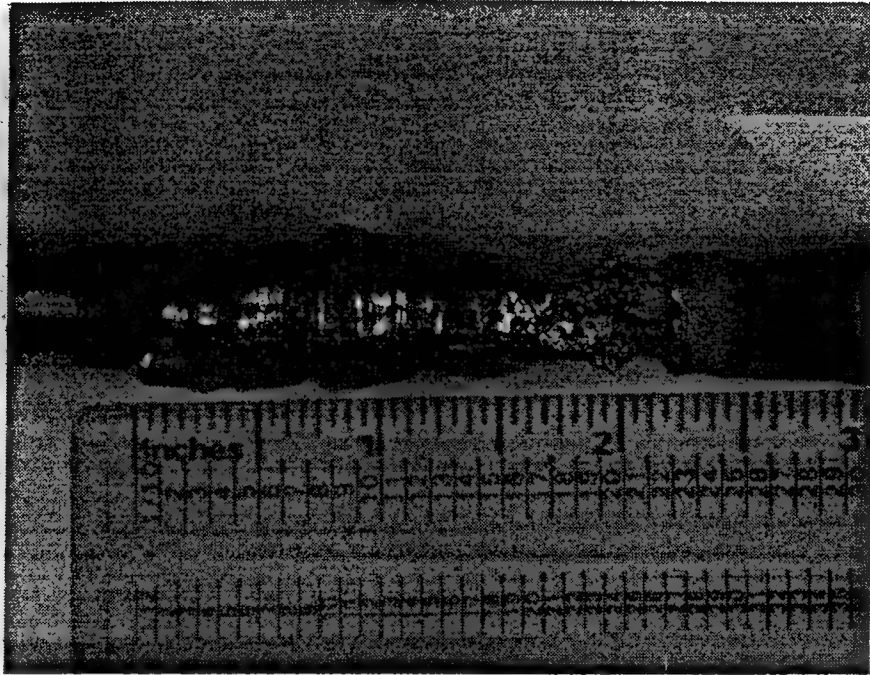


Figure 8. Float zone attempt with 86% W CIP rod.



Figure 9. Ingot #4, sintered and float zoned 93% W CIP rod-  
travel down page. 100X

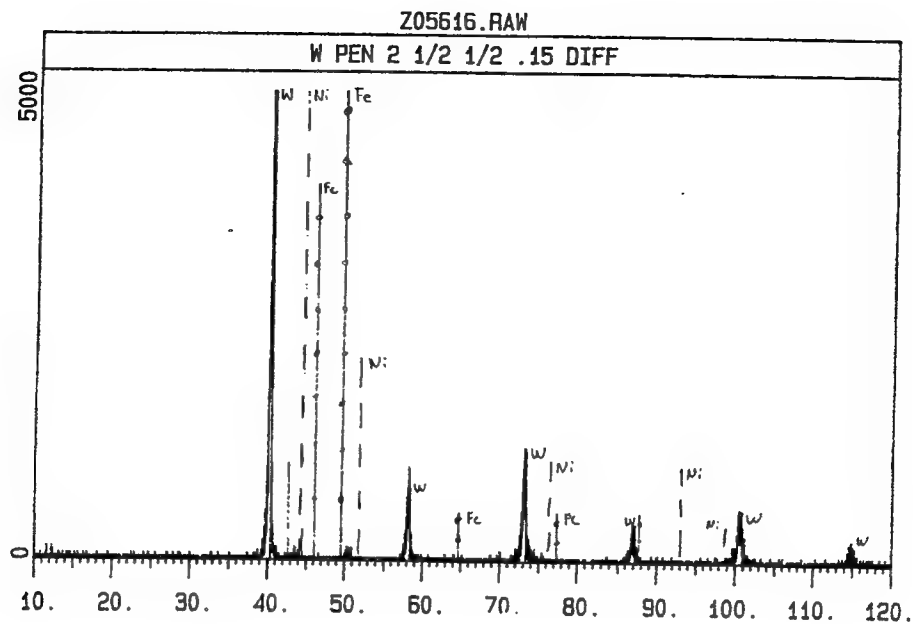


Figure 10. X-ray diffraction of tip of ingot #4.

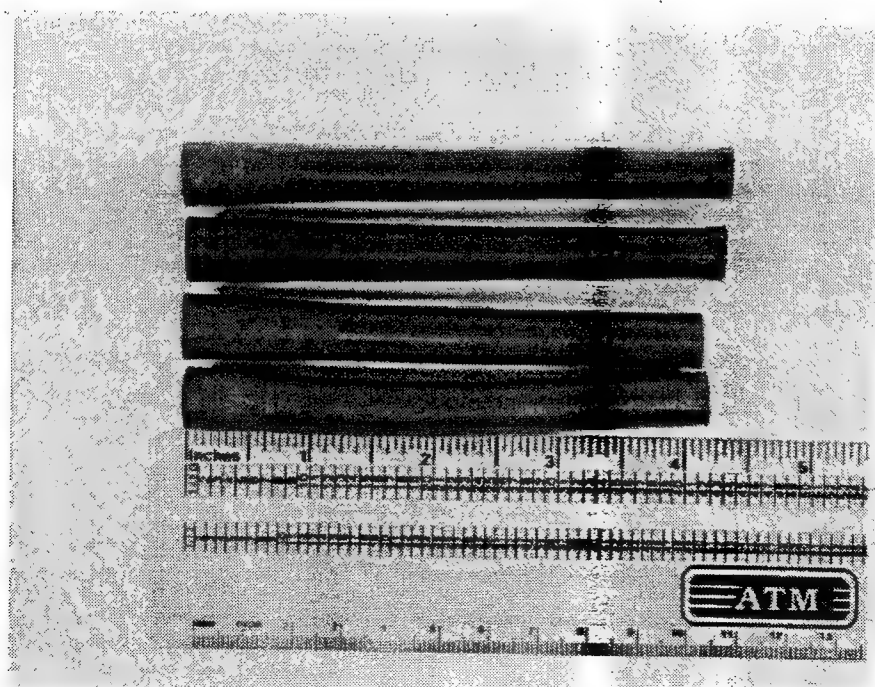


Figure 11. Ingots of 93% W sintered & float zoned before EDM- bottom is #4.

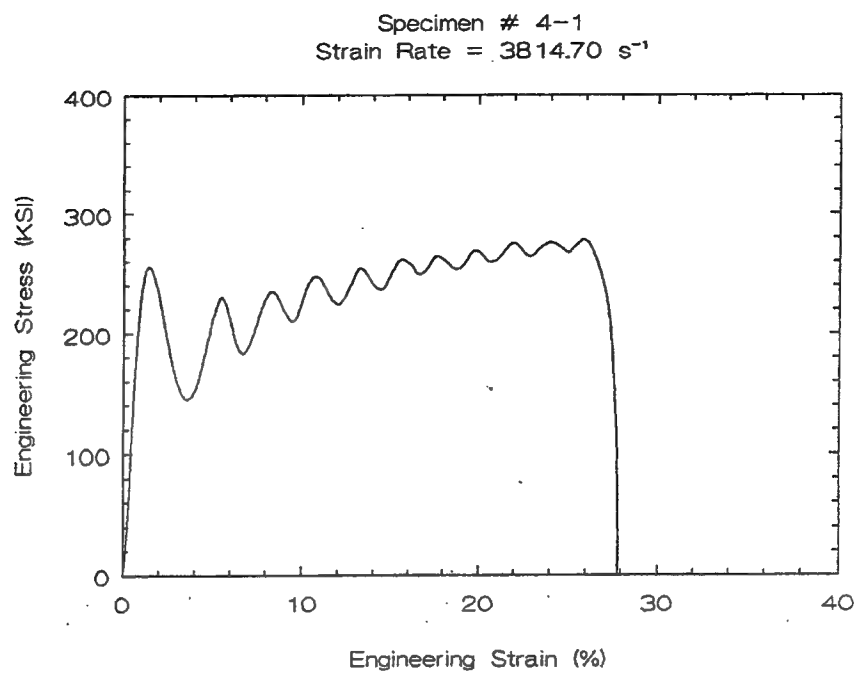


Figure 12a. Compression sample 4-1- made from ingot #4

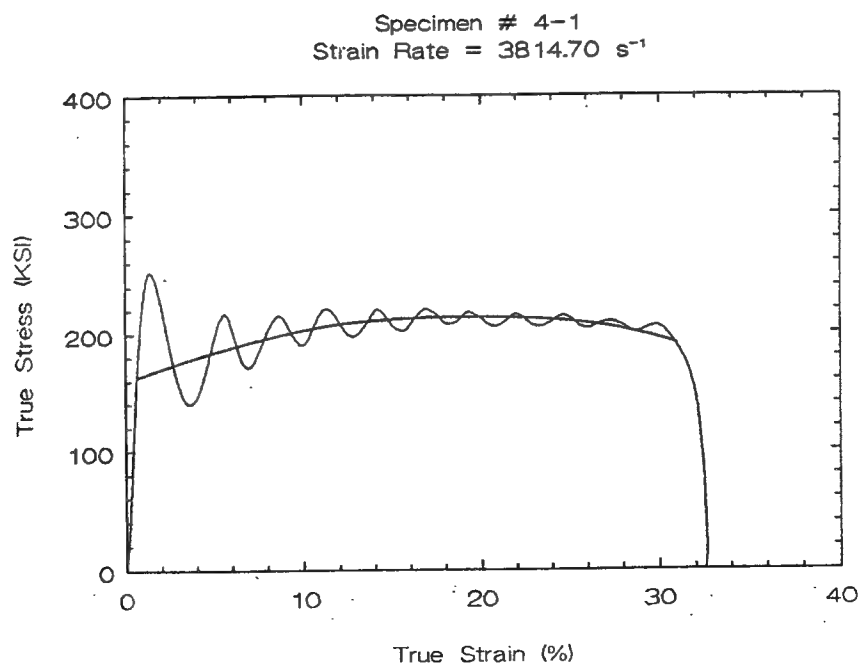


Figure 12b. Compression sample 4-1- made from ingot #4.

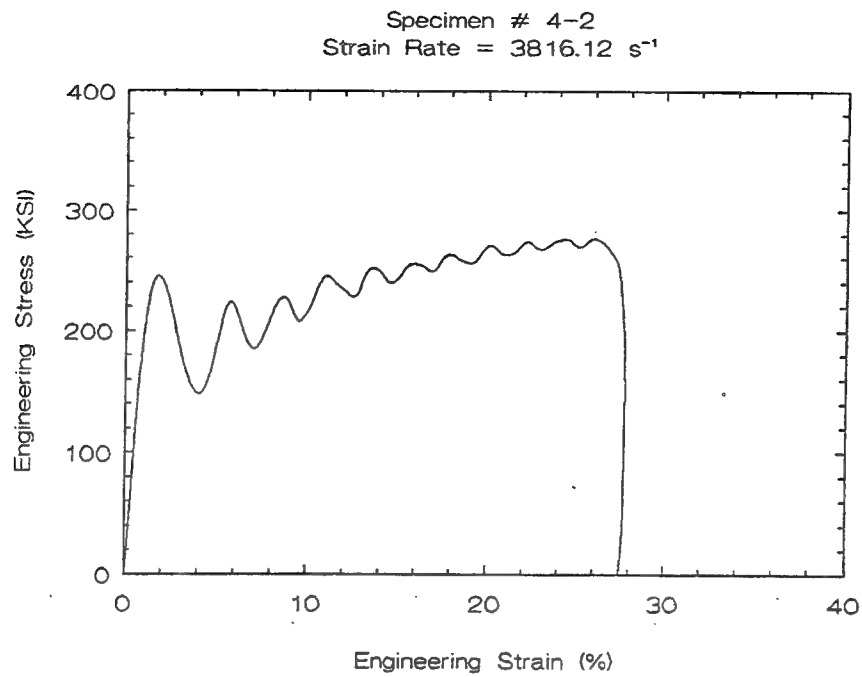


Figure 12c. Compression sample 4-2- made from ingot #4.

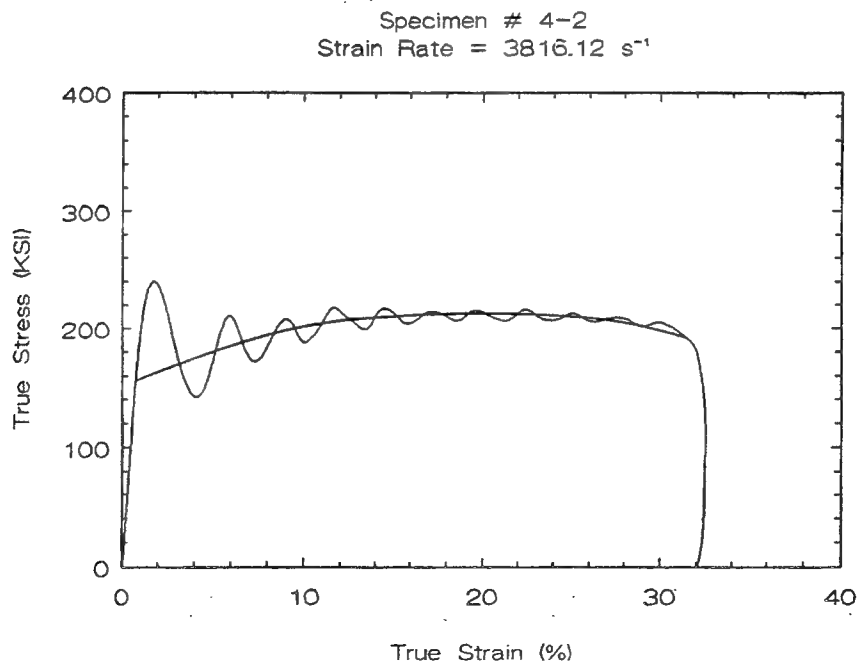


Figure 12d. Compression sample 4-2- made from ingot #4.

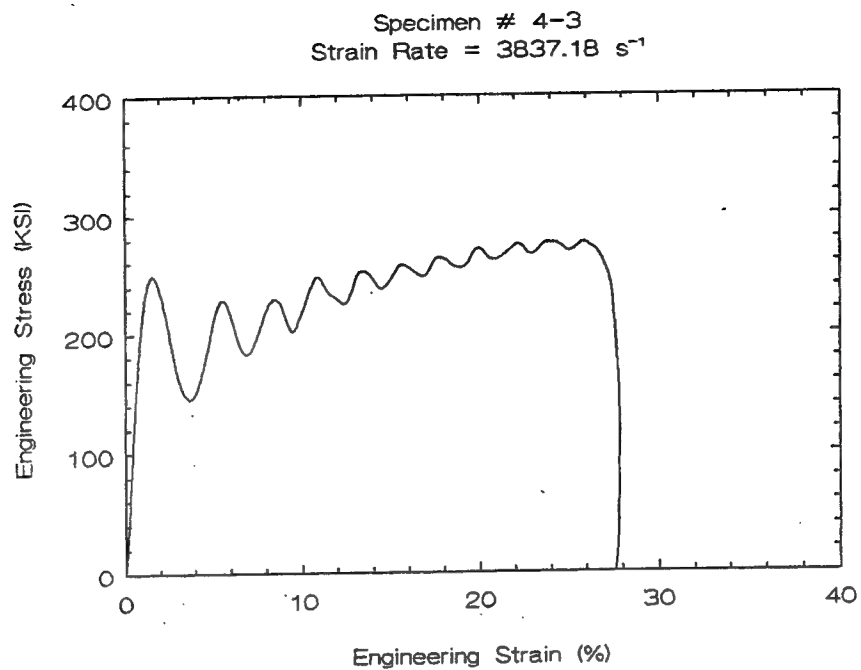


Figure 12e. Compression sample 4-3- made from ingot #4.

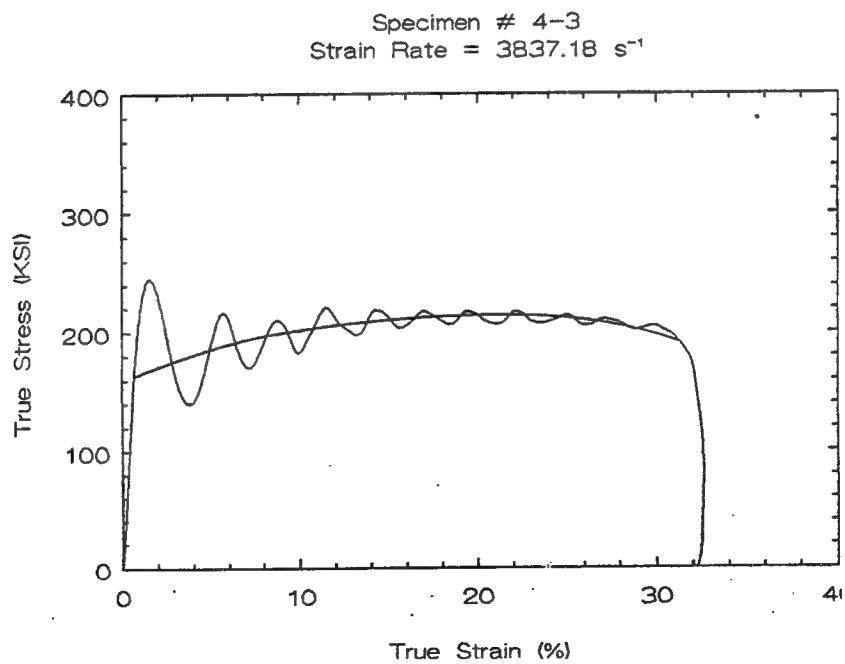


Figure 12f. Compression sample 4-3- made from ingot #4.

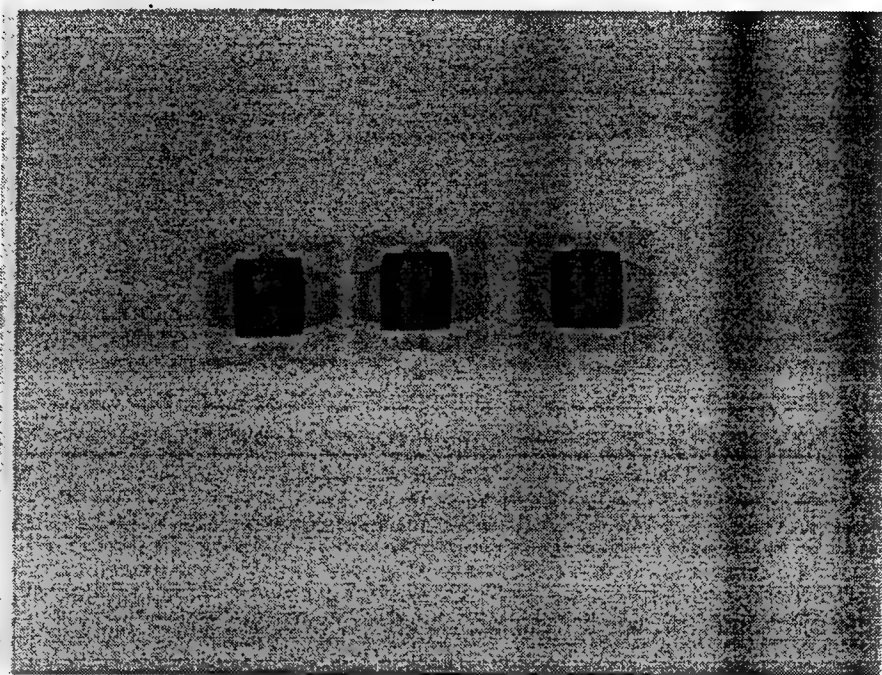


Figure 13. Samples 4-1, 4-2, 4-3 after compression testing.



Figure 14. Ingot 2W, float zoned W rod with Ni-Fe molten zone. 100X.  
Travel down the page.

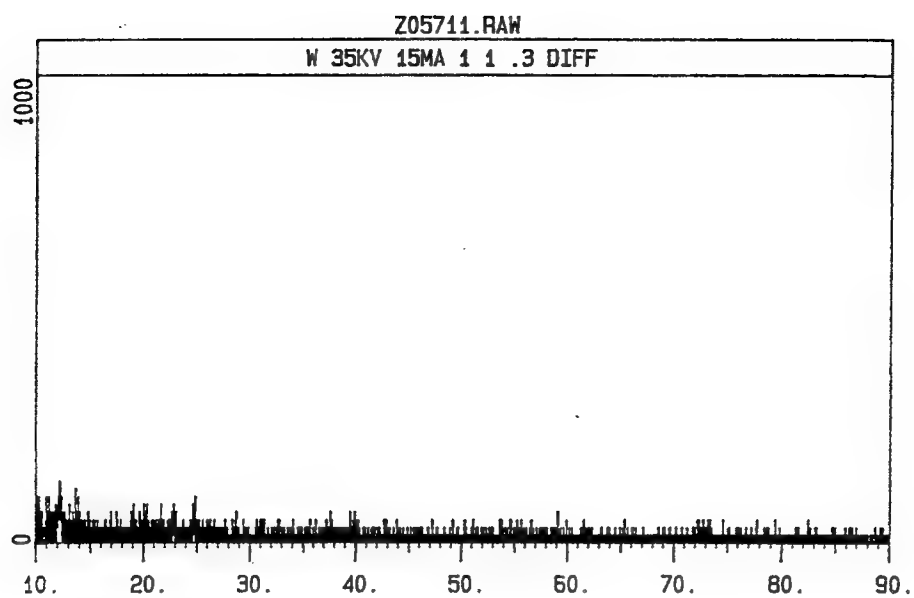


Figure 15a. X-ray diffraction ingot 2W center of tip.

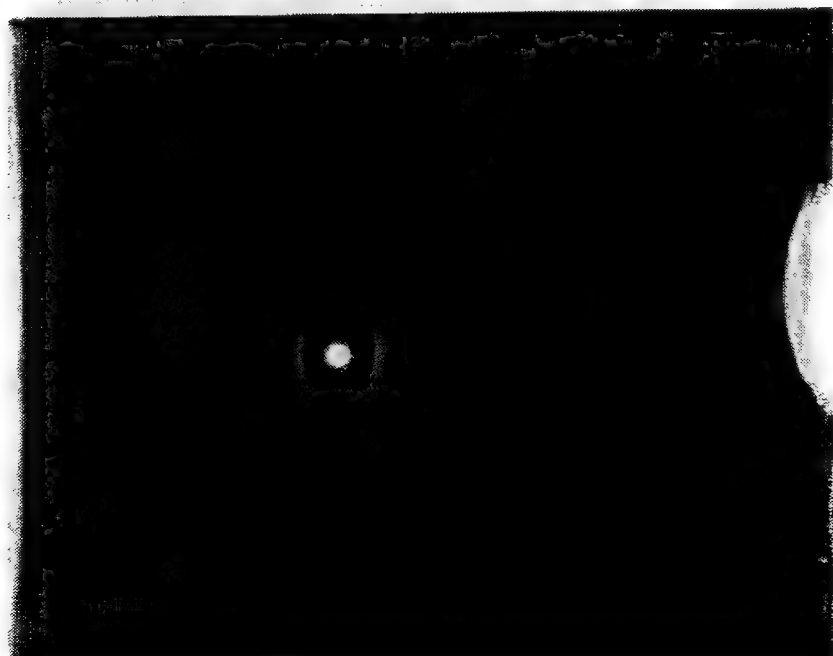


Figure 15b. Laue pattern ingot 2W.

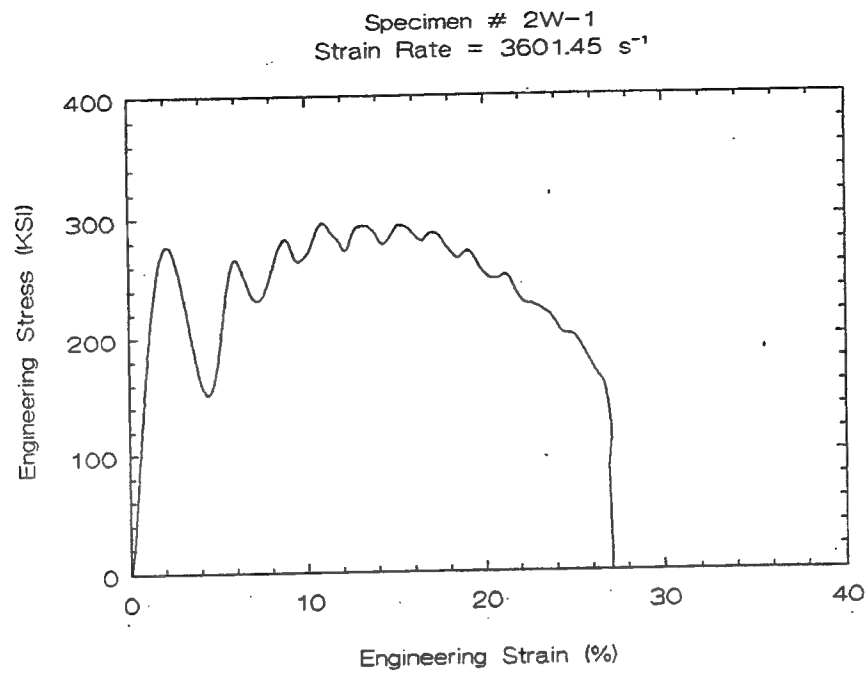


Figure 16a. Compression sample 2W-1- made from ingot 2W.

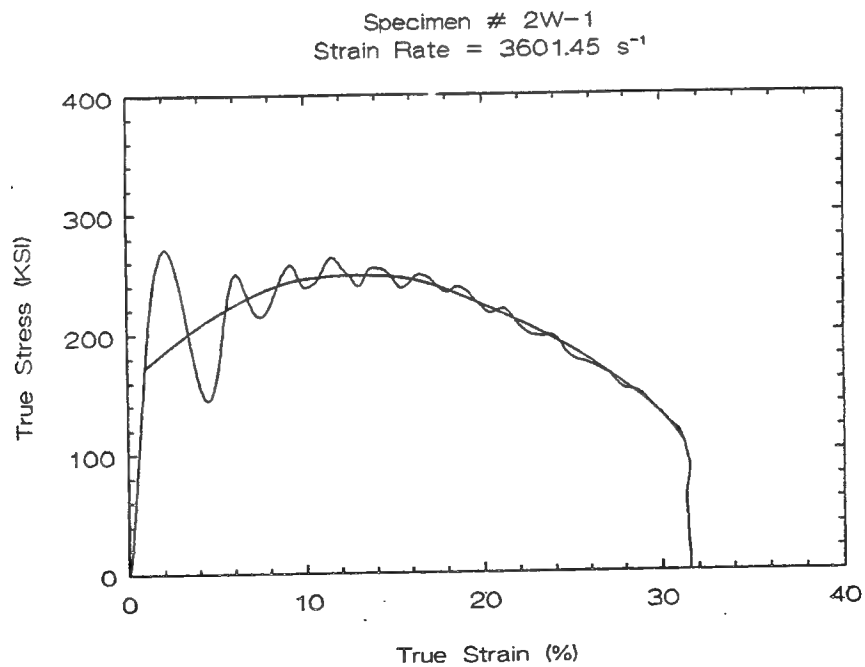


Figure 16b. Compression sample 2W-1- made from ingot 2W.

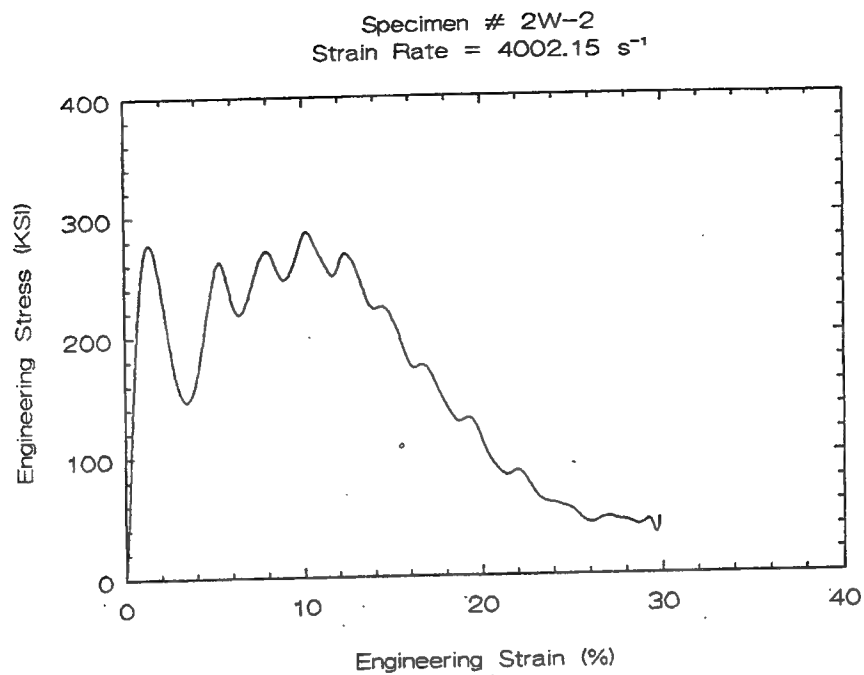


Figure 16c. Compression sample 2W-2- made from ingot 2W.

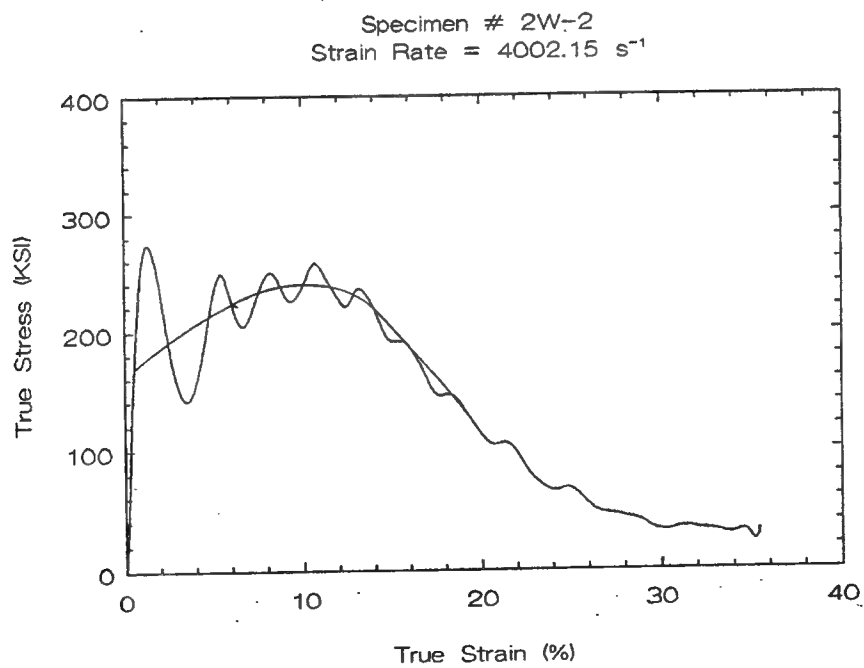


Figure 16d. Compression sample 2W-2- made from ingot 2W.

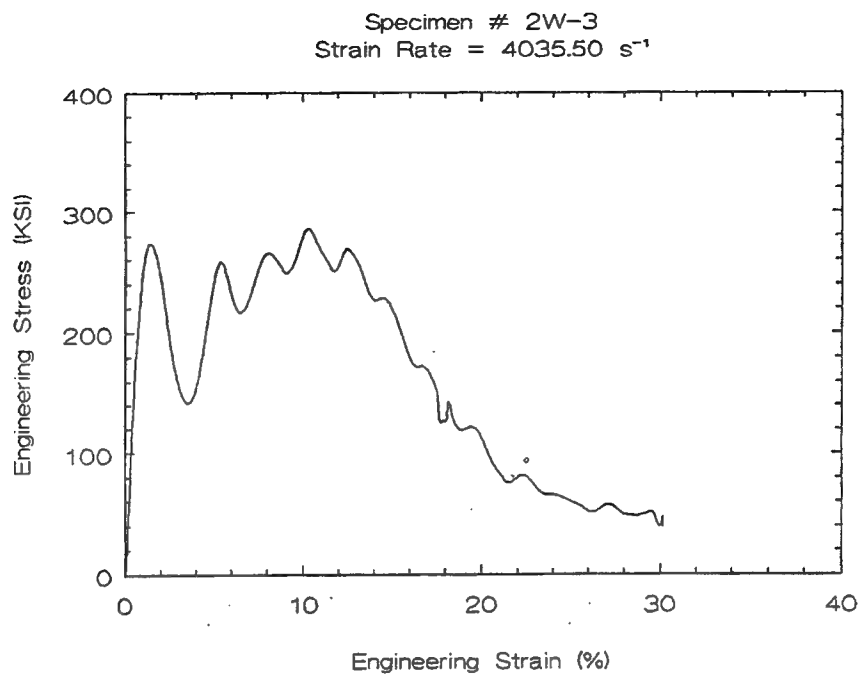


Figure 16e. Compression sample 2W-3- made from ingot 2W.

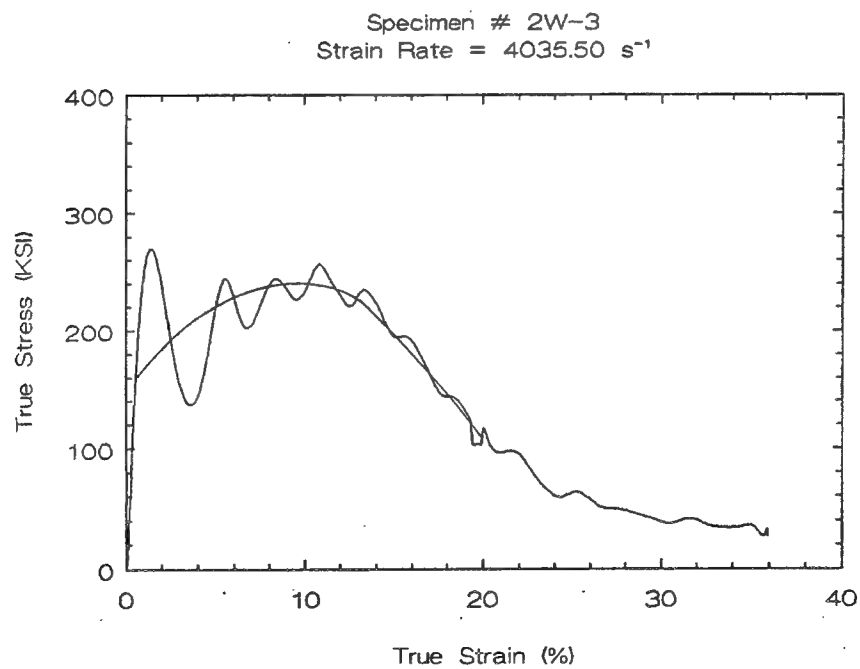


Figure 16f. Compression sample 2W-3- made from ingot 2W.

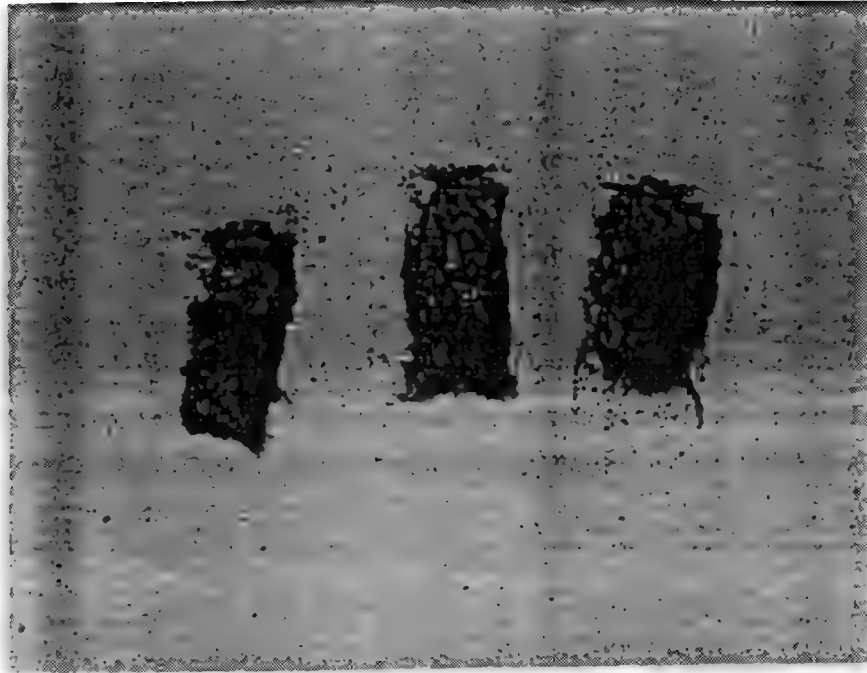


Figure 17. Samples 2W-1, 2W-2, 2W-3 after compression testing.



Figure 18. Ingots made by sintering & float zoning CIP rods with 5% Re.  
2R is top.

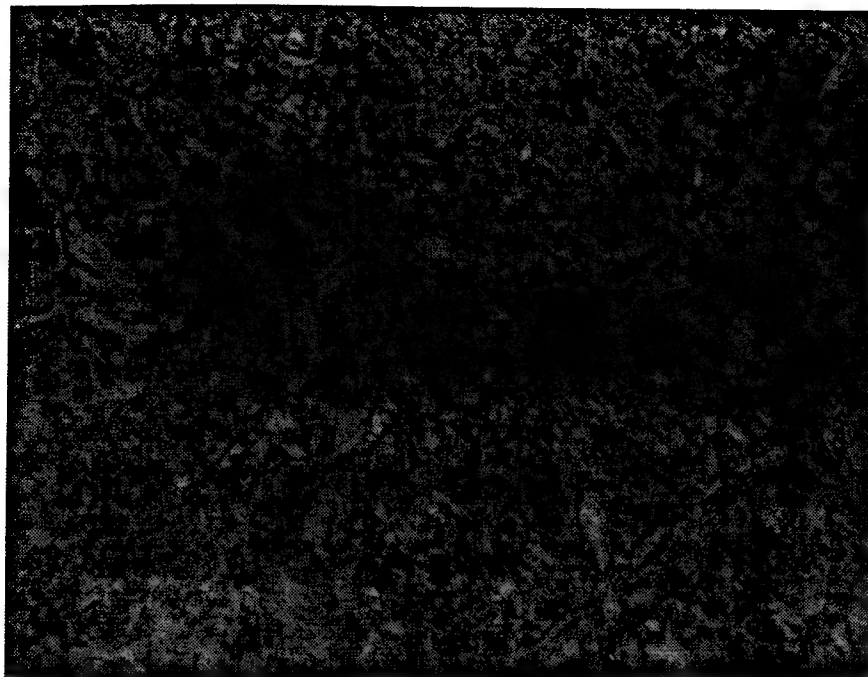


Figure 19. Center of tip of ingot 2R- travel is down the page. 100X.

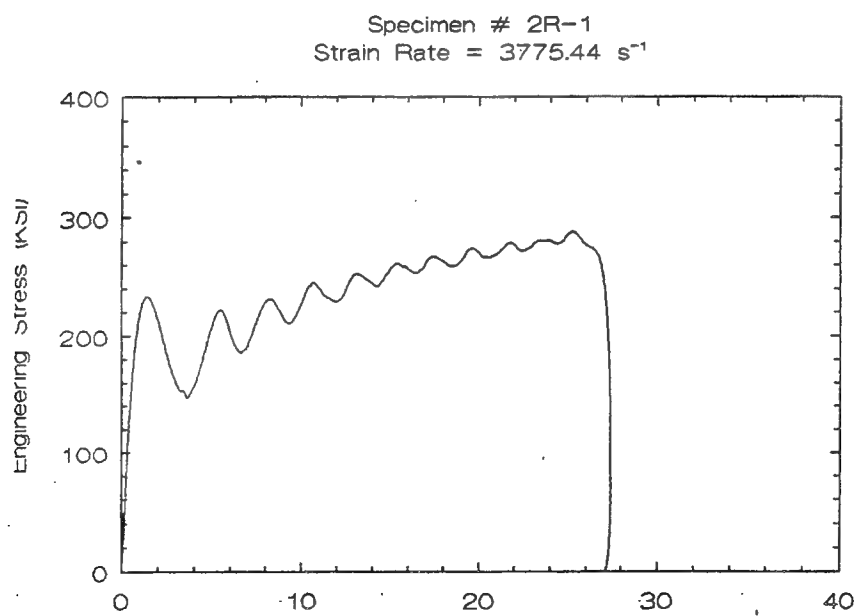


Figure 20a. Compression sample 2R-1- made from ingot 2R.

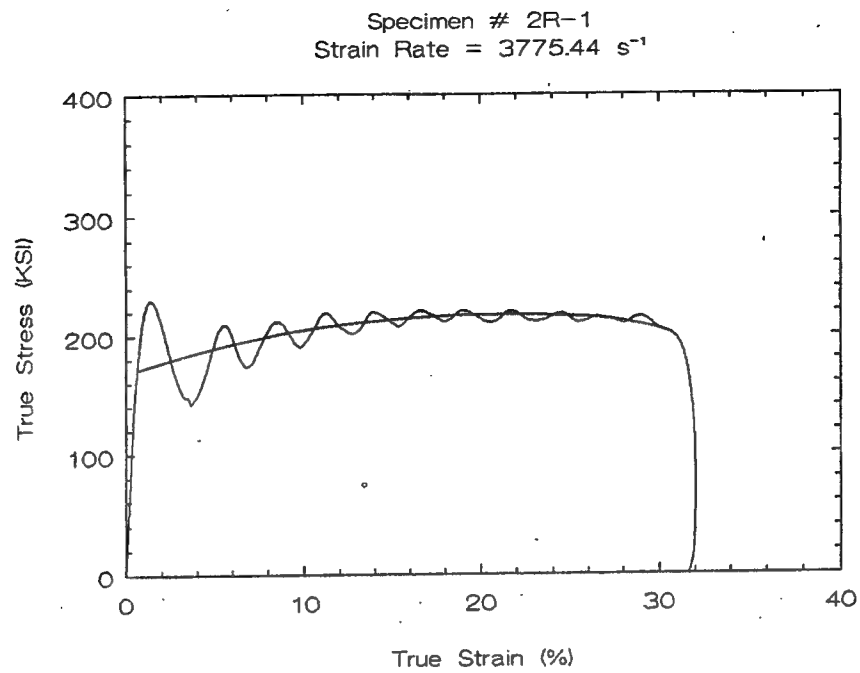


Figure 20b. Compression sample 2R-1- made from ingot 2R.

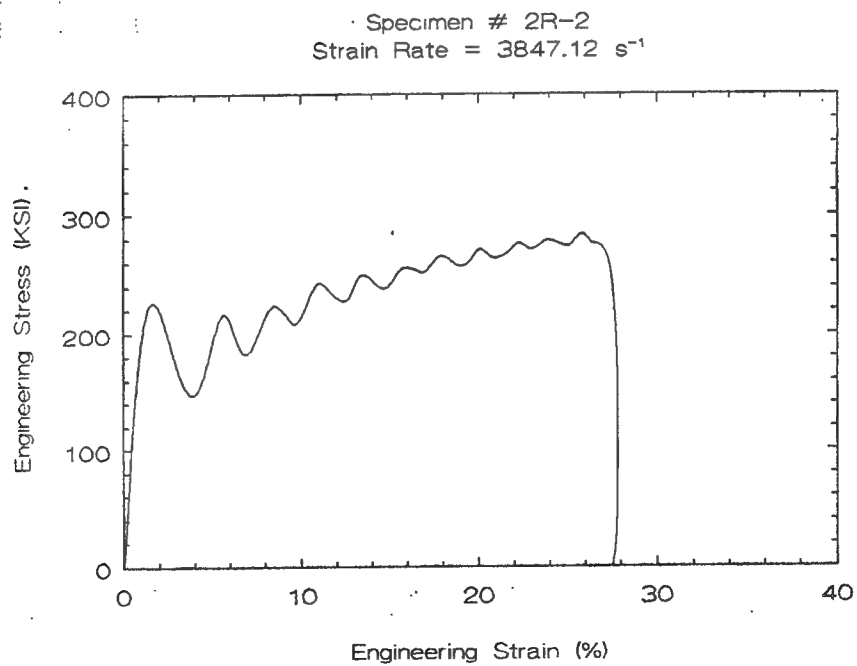


Figure 20c. Compression sample 2R-2- made from ingot 2R.

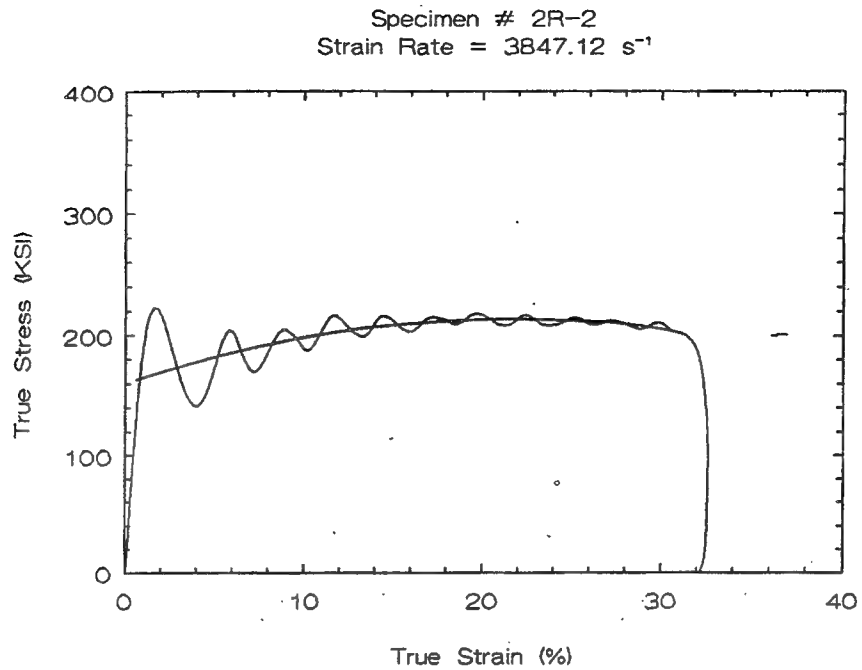


Figure 20d. Compression sample 2R-2- made from ingot 2R.

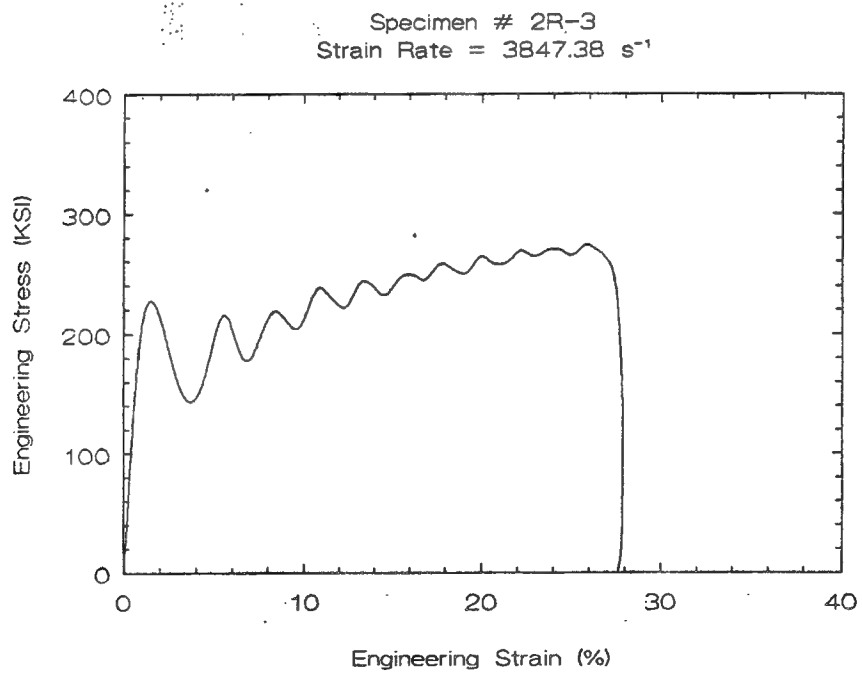


Figure 20e. Compression sample 2R-3- made from ingot 2R.

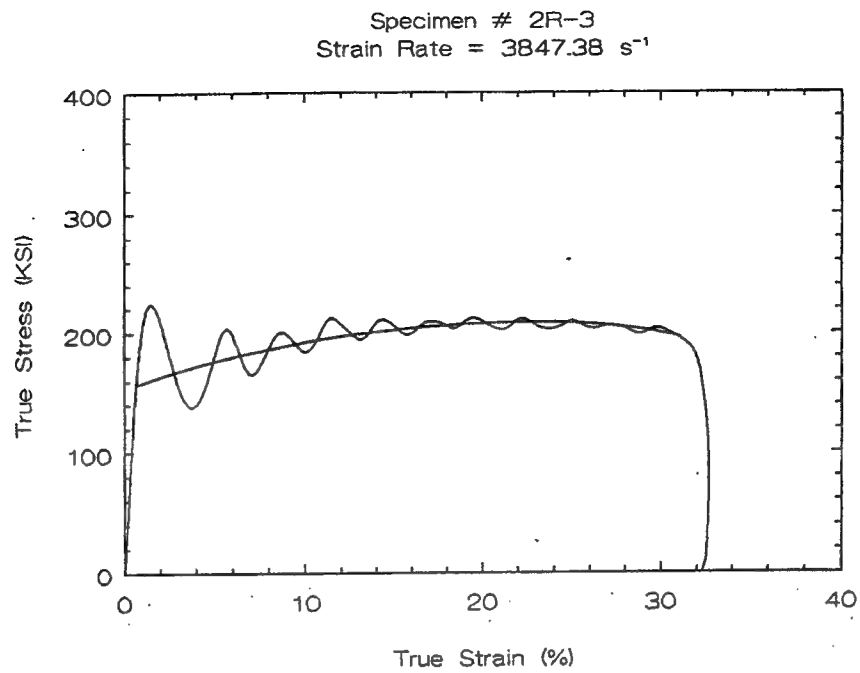


Figure 20f. Compression sample 2R-3- made from ingot 2R.

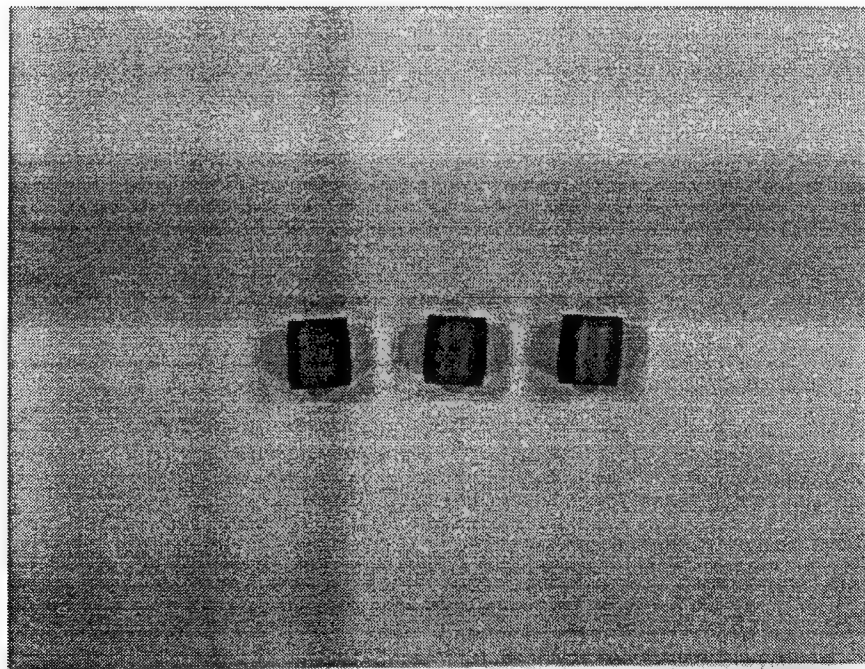


Figure 21. Sample 2R-1, 2R-2, 2R-3 after compression testing.

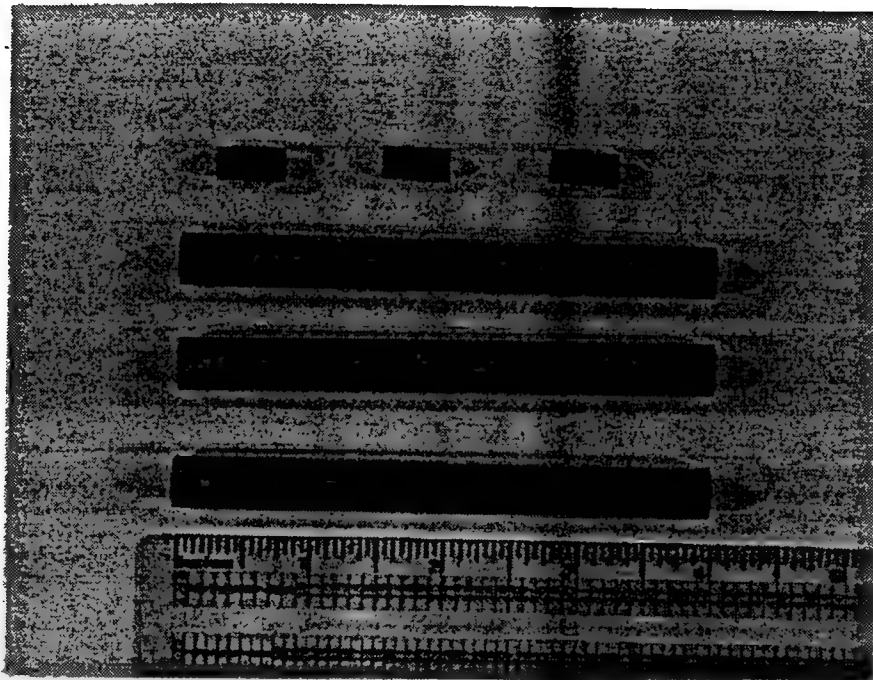


Figure 22a. Compression and ballistic samples- 93% W CIP rods after EDM.

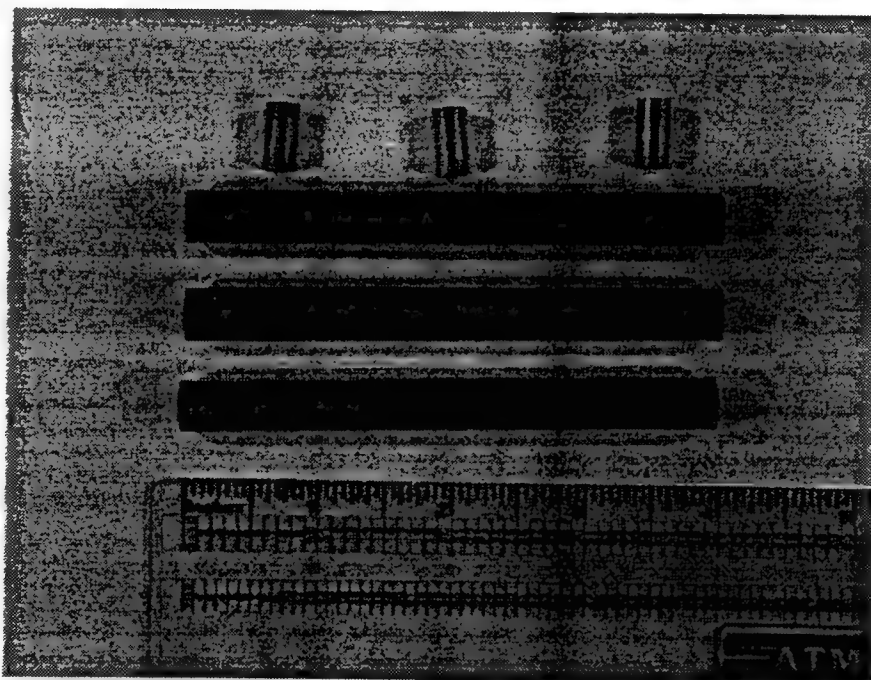


Figure 22b. Compression & ballistic samples from W-Re CIP rods after EDM.

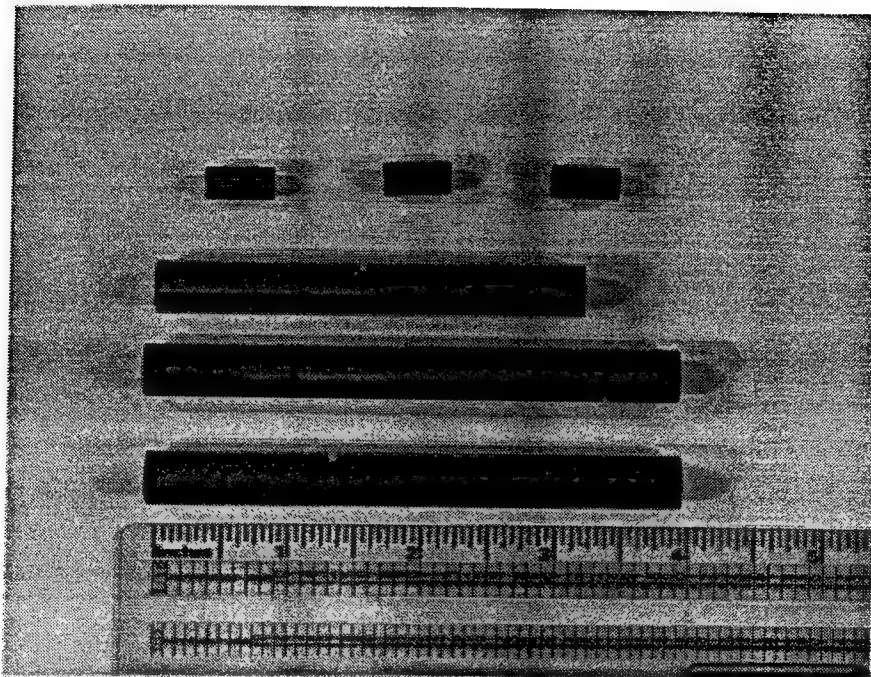


Figure 22c. Compression and ballistic samples, pure W rods after EDM.  
Note slots.

## Distribution List

1 Office of the Secretary of Defense for Research and Engineering, The Pentagon,  
Washington, D.C. 20301

Director, U.S. Army Research Laboratory, 2800 Powder Mill Road, Adelphi, MD 20783-1197

1 ATTN: AMSRL-OP-SD-TP, Technical Publishing Branch  
1 Dr. Alan Goldman  
1 AMSRL-OP-SD-TA, Records Management Administrator  
1 AMSRL-OP-SD-TL, Technical Library

Commander, Defense Technical Information Center, Cameron Station, Building 5, 5010 Duke  
Street, Alexandria, VA 22304-6145

2 DTIC-FDAC

1 MIAC/CINDAS, Purdue University, 2595 Yeager Road, West Lafayette, IN 47905

Commander, Army Research Office, P.O. Box 12211, Research Triangle Park, NC  
27709-2211

1 ATTN: Information Processing Office  
1 Dr. Andrew Crowson  
1 Dr. Edward Chen  
1 Dr. K. Iyer

Commander U.S. Army Materiel Command (AMC), 5001 Eisenhower Avenue, Alexandria, VA  
22333

1 ATTN: AMCSCI

Commander, U.S. Army Materiel Systems Analysis Activity, Aberdeen Proving Ground, MD  
21005

1 ATTN: AMXSY-MP, Director

Commander, U.S. Army Missile Command, Redstone Arsenal, AL 35809

1 ATTN: AMSMI-RD-CS-R/Doc  
Al Ingram, AMSMI-RD-ST-CM

Commander, U.S. Army Armament Research Development and Engineering Center, Dover, NJ  
07801

1 ATTN: Technical Library  
1 Mr. D. Kapoor  
1 Dr. S. Cytron  
1 Mr. K. Willison  
1 Dr. J. Pearson  
1 Dr. E. Baker  
1 Dr. W. Ebihara

Commander, U.S. Army Tank-Automotive Command, Warren, MI 48397-5000  
2 ATTN: AMSTA-TSL Technical Library

Commander, U.S. Army Foreign Science and Technology Center, 220 7th Street, N.E.,  
Charlottesville, VA 22901  
3 ATTN: AIFRTC, Applied Technologies Branch, Gerald Schlesinger

Naval Research Laboratory, Washington, D.C. 20375

1 ATTN: Code 62  
1 Dr. Virgil Provenzano  
1 Dr. Jack Ayers  
1 Dr. B. B. Rath

Chief of Naval Research, Arlington, VA 22217

1 ATTN: Code 471  
1 Dr. A.K. Vasudevan  
1 Dr. George Yoder

Naval Surface Weapons Center, Dahlgren Laboratory, Dahlgren, VA 22448

1 ATTN: Code G-32, Ammunition Branch, Mr. Peter Adams

Commander, Rock Island Arsenal, Rock Island, IL 61299-6000

1 ATTN: SMCRI-SEM-T

Battelle Columbus Laboratories, Battelle Memorial Institute, 505 King Avenue, Columbus, OH 43201

1 ATTN: Mr. Henry Cialone  
1 Dr. Alan Clauer

Battelle Pacific Northwest Laboratories, P.O. Box 999, Richland, WA 99352

1 ATTN: Mr. William Gurwell  
1 Dr. Gordon Dudder  
1 Mr. Curt Lavender  
1 B. Armstrong

Osram Sylvania, Inc. Chemical and Metallurgical Division, Hawes Street, Towanda, PA 18848

1 ATTN: Dr. James Mullendore  
1 Mr. James Spencer  
1 Ms. Susan Doecker  
1 Mr. David Houck

Director, U.S. Army Research Laboratory, Aberdeen Proving Ground, MD 21005

1 ATTN: AMSRL-WT  
1 AMSRL-WT-T, Dr. Lee Magness  
1 AMSRL-WT-T, Ms. W.A. Leonard  
1 AMSRL-WT-T, Dr. W. de Rosset  
1 AMSRL-WT-T, Dr. W. Morrison  
1 AMSRL-WT, Dr. A. Dietrich

Teledyne Advanced Materials 1 Teledyne Place, LaVergne, TN 37086

1 ATTN: Dr. Steven Caldwell  
1 Mr. James Oakes

Los Alamos National Laboratory, ATAC, MS F681, P.O. Box 1663, Los Alamos, NM 87545

1 ATTN: Mr. Bill Hogan  
1 Mr. Paul Dunn  
1 Mr. Bill Baker  
1 Dr. George T. Gray III  
1 Ms. Sherri Bingert

Philips Elmet, 1560 Lisbon Road, Lewiston, ME 04240

1 ATTN: Mr. James Anderson

Ultramet, Inc., 12173 Montague Street, Pacoima, CA 91331

1 ATTN: Mr. Brian Williams  
1 Dr. Robert Tuffias  
1 Mr. A. Sherman

Ceracon, Inc., 1101 N. Market Boulevard, Suite 9, Sacramento, CA 95834

1 ATTN: Dr. Ramas Raman  
1 Mr. Sundeep Rele

Southwest Research Institute, 6220 Culebra Road, P.O. Drawer 28510, San Antonio, TX 78228-0510

1 ATTN: Dr. James Lankford  
1 Dr. Hervé Couque  
1 Dr. Charles Anderson

Metalworking Technology, Inc., 1450 Scalp Avenue, Johnstown, PA 15904

1 ATTN: Mr. C. Buck Skena  
1 Mr. Timothy McCabe

Research Triangle Institute, P.O. Box 12194, Research Triangle Park, NC 27709-2154

1 ATTN: Dr. John B. Posthill

3C Systems, 620 Arglye Road, Wynnewood, PA 19096

1 ATTN: Mr. Murray Kornhauser

Advance Technology Coatings, 300 Blue Smoke Ct. West, Fort Worth, TX 76105

1 ATTN: Dean Baker

Alliant Techsystems, 7225 Northland Drive, Brooklyn Park, MN 55428

1 ATTN: Dr. Stan Nelson

1 Mr. Mark Jones

SPARTA, Inc., CAMDEC Division, 2900-A Saturn Street, Brea, CA 92621-6203

1 ATTN: John A. Brinkman

Defense Technology International, Inc., The Stark House, 22 Concord Street,  
Nashua, NH

1 ATTN: Mr. Douglas Ayer

Materials and Electrochemical Research Corporation, 7960 S. Kolb Road, Tucson, AZ 85706

1 ATTN: Dr. James Withers

1 Dr. Sumit Guha

Materials Modification, Inc., 2929-P1 Eskridge Center, Fairfax, VA 22031

1 ATTN: Dr. T.S. Sudarshan

Dr. S. Raghunathan

Micro Materials Technology, 120-D Research Drive, Milford, CT 06460

1 ATTN: Dr. Richard Cheney

Nuclear Metals, 2229 Main Street, Concord, MA 01742

1 ATTN: Dr. William Nachtrab

Olin Ordnance, 10101 9th Street N., St. Petersburg, FL

1 ATTN: Hugh McElroy

The Pennsylvania State University, Department of Engineering Science and Mechanics, 227  
Hammond Building, University Park, PA 16802-1401

1 ATTN: Dr. Randall M. German, Professor, Brush Chair in Materials

Worcester Polytechnic Institute, 100 Institute Road, Worcester, MA, 01609

1 ATTN: Dr. Ronald Biederman

1 Dr. Richard Sisson

1 Dr. Chickery Kasouf

1 Dr. David Zenger

Failure Analysis Associates, Inc., 149 Commonwealth Drive, PO Box 3015, Menlo Park, CA 94025

1 ATTN: S.P. Andrew  
1 R.D. Caliguri  
1 T.K. Parnell  
1 L.E. Eiselstein

Amorphous Technologies International, Laguna Hills, CA

1 ATTN: Mr. Dick Harlow

Parmatech Corporation, 2221 Pine View Way, Petaluma, CA 94952

1 ATTN: Dr. Animesh Bose

Stiglich Associates, PO Box 206, Sierra Madre, CA 91025

1 ATTN: Dr. Jack Stiglich

Northwestern University, Department of Engineering Sciences and Applied Mathematics,  
Evanston, IL 60208

1 ATTN: Dr. W. Edward Olmstead

Michigan Technological University, Department of Mechanical Engineering and Engineering  
Mechanics, 1400 Townsend Drive, Houghton, MI 49931-1295

1 ATTN: Dr. Subhash Ghatuparthi

Naval Surface Warfare Center, 10901 New Hampshire Avenue, Silver Spring, MD 20903-5000

1 ATTN: Mr. Robert Garrett  
1 Mr. A.P. Divecha  
1 Mr. S. Karmakar

IAP Research Inc., 2763 Culver Avenue, Dayton, OH, 45429-3723

1 ATTN: Dr. Bhanu Chelluri

Valenite, 1711 Thunderbird Drive, Troy, MI 48084

1 ATTN: Dr. D.G. Bhat

California Institute of Technology, Graduate Aeronautical Laboratories, Pasadena, CA 91125

1 ATTN: Dr. G. Ravichandran  
1 Dr. William Johnson

Sandvik Rhenium Alloys, 1329 Taylor Street, PO Box 245, Elyria, OH, 44038-0245

1 ATTN: Dr. Boris Bryskin

University of California-Davis, EU-II, Davis, CA, 95616

1 ATTN: Dr. Joanna Groza  
1 Dr. Subhash Risbud

Forged Performance Products Inc., 277 Warehouse Road, Oak Ridge, TN 37830

1 ATTN: Mr. Ed Hodge  
1 Mr. Hubert Tarenner

Superior Graphite, 120 South Riverside Plaza, Chicago, IL 60606

1 ATTN: Dr. William Goldberger  
1 Mr. Brian Merkle

Georgia Institute of Technology, Department of Materials Engineering, Atlanta, GA 30332

1 ATTN: Dr. Naresh Thadhani

ARPA, 3701 North Fairfax Drive, Arlington, VA 22203-1714

1 ATTN: Dr. B. Wilcox  
1 Dr. R. Crowe

University of Idaho, Institute for Materials and Advanced Processes, Office of the Director, Mines Building, Room 204, Moscow, Idaho, 83844-3026

1 ATTN: Dr. F. H. Froes

National Institute of Standards and Technology, Gaithersburg, MD 02899

1 ATTN: Dr. Subhas Malghan

Johns Hopkins University, Whiting School of Engineering, 3400 N. Charles Street, Baltimore, MD 21218-2686

1 ATTN: Dr. K. T. Ramesh  
1 Dr. William Sharpe, Jr.  
1 Dr. James Spicer  
1 Dr. Kevin Hemker  
1 Dr. Gang Bao  
1 Dr. James Wagner

Martin Marietta Energy Systems, Oak Ridge National Laboratory, Oak Ridge, TN 37831-6083

1 ATTN: Dr. Vinod Sikka  
1 Dr. Evan Ohriner  
1 Dr. Gail Mackiewicz-Ludtka

Director, U.S. Army Research Laboratory, Watertown, MA 02172-0001

2 ATTN: AMSRL-OP-CI-D, Technical Library  
1 AMSRL-OP-PR-WT  
20 AMSRL-MA-CB, Authors

revised March 13, 1995